

Submitted to AJ; R1 10/05/2015

Kepler Eclipsing Binaries with Stellar Companions

D. R. Gies, R. A. Matson, Z. Guo, K. V. Lester

Center for High Angular Resolution Astronomy and Department of Physics and Astronomy, Georgia State University, P. O. Box 5060, Atlanta, GA 30302-5060, USA

gies@chara.gsu.edu, rmatson@chara.gsu.edu, guo@chara.gsu.edu,
lester@chara.gsu.edu

J. A. Orosz

Department of Astronomy, San Diego State University, San Diego, CA 92182-1221, USA

jorosz@mail.sdsu.edu

and

G. J. Peters

Space Sciences Center and Department of Physics and Astronomy, University of Southern California, Los Angeles, CA 90089-1341, USA

gjpeters@mucen.usc.edu

ABSTRACT

Many short-period binary stars have distant orbiting companions that have played a role in driving the binary components into close separation. Indirect detection of a tertiary star is possible by measuring apparent changes in eclipse times of eclipsing binaries as the binary orbits the common center of mass. Here we present an analysis of the eclipse timings of 41 eclipsing binaries observed throughout the NASA *Kepler* mission of long duration and precise photometry. This subset of binaries is characterized by relatively deep and frequent eclipses of both stellar components. We present preliminary orbital elements for seven probable triple stars among this sample, and we discuss apparent period changes in seven additional eclipsing binaries that may be related to motion about a tertiary in a long period orbit. The results will be used in ongoing investigations of the spectra and light curves of these binaries for further evidence of the presence of third stars.

Subject headings: binaries (including multiple): close — binaries: eclipsing — starspots — stars: formation — techniques: photometric

1. Introduction

The process of star formation involves a large scale transfer of angular momentum from inner cloud to outer disk that often results in the formation of binary stars (Duchêne & Kraus 2013). The reduction in separation to produce close pairs may involve the action of a third star through the eccentric Kozai-Lidov mechanism (Naoz & Fabrycky 2014), and indeed Tokovinin et al. (2006) showed that most short period binaries are orbited by a distant third star (96% for $P < 3$ days). Such tertiary companions can be directly observed in nearby cases through high angular resolution methods, but for most binaries we need other means to detect them. A particularly attractive method is to search for light travel time effects in the times of minima of eclipsing binaries that are caused by the displacement of the binary around the center of mass of the binary - tertiary system (Mayer 1990; Pribulla et al. 2005).

The NASA *Kepler* mission has provided us with a singular opportunity to search for eclipse timing variations due to orbital motion about a third star. The *Kepler* and follow-on *K2* missions have created long duration light curves¹ for some 3000 eclipsing binaries (Prša et al. 2011; Slawson et al. 2011; Armstrong et al. 2015; LaCourse et al. 2015). The search for eclipse time variations among the *Kepler* binaries has been led by Conroy et al. (2014) (short period systems through Q16) and Orosz (2015) (long period systems). These surveys indicate that $\approx 18\%$ of the observed systems display variations consistent with orbital motion about a third star. Detailed case studies of specific triples have been presented by Rappaport et al. (2013), Borkovits et al. (2015), and Zasche et al. (2015), among others. Furthermore, *Kepler* light curves have uncovered a number of remarkable cases in which the orientation of the outer system is such that eclipses by the tertiary are also observed (Carter et al. 2011; Drekas et al. 2011; Armstrong et al. 2012; Borkovits et al. 2013).

We embarked on a search for eclipse timing variations among a subset of 41 eclipsing binaries that were identified prior to the start of *Kepler* observations (Gies et al. 2012). We subsequently completed a large set of spectroscopic observations of this sample in order to derive spectroscopic orbital elements, estimate the stellar properties, compare with evolutionary codes, and explore the pulsational properties of the component stars. Our first paper documented the eclipse times in observations made over quarters Q0 – Q9 (2009.3 – 2011.5). Now with the *Kepler* mission complete with observations through Q17 (ending

¹<http://keplerebs.villanova.edu/>

2013.4), we present here the eclipse timings for our sample of 41 binaries over the entire duration of the mission. These results help document the frequency of tertiary companions in this well-observed group of stars and provide period, epoch, and third-light constraints for our ongoing spectroscopic and light curve analyses. We present the full set of timing measurements in Section 2, and we offer preliminary orbital elements for seven probable triple systems in Section 3. We summarize the results and discuss their implications in Section 4.

2. Eclipse Timing Measurements

The *Kepler* light curves of the target eclipsing binaries represent the latest reprocessing of all the observations made between quarters Q0 and Q17. These are long cadence measurements that are obtained in net exposure times of 29.4244 minutes. The associated times given in our first paper (Gies et al. 2012) were based upon UTC (Coordinated Universal Time) while the current set uses TDB (Barycentric Dynamical Time²), and here we report the times in reduced Barycentric Julian Date (BJD – 2,400,000 days). We used the Simple Aperture Photometry (SAP) flux except in the case of KIC 04678873. This star has a nearby companion that creates large variations in the summed flux throughout and between observing quarters. We used PyKE³ software to extract the flux of this target using a larger aperture that included both stars. The final light curve has a significant “third light” flux contribution from the companion but is free from large fluctuations between quarters. These light curves were detrended as described in our first paper, and the subsequent analysis is based on flux versions normalized to unity at the maximum between eclipses. The list of targets appears in Table 1.

The eclipse timing measurements were made in almost the same way as described in our first paper. We first formed an eclipse template as a function of orbital phase by assuming a preliminary eclipse epoch T and binary orbital period P and then forming a phase rebinned version of the specific primary or secondary eclipse from all the available fluxes. The template was then smoothed by convolution with a Gaussian function to avoid the introduction of spurious patterns in systems where the orbital period is a near integer multiple of the observational cadence (Conroy et al. 2014). The eclipse template was recentered on the minimum by fitting a parabola to the lowest 20% of the eclipse flux, and the epoch of minimum adjusted accordingly. We then fit the template to each eclipse (after local flux normalization) using the code MPFIT (Markwardt 2009) to find best match with parameters

²https://archive.stsci.edu/kepler/release_notes/release_notes19/DataRelease_19_20130204.pdf

³<http://keplerscience.arc.nasa.gov/DataAnalysisTools.shtml>

for the phase offset and an eclipse depth scaling factor D_E . The latter parameter allows the eclipse template to be transformed by

$$F(\text{revised}) = 1 - D_E + D_E F(\text{template}) \quad (1)$$

so that temporal changes in the eclipse depth may be tracked. The eclipse depth changes are interesting in the context of long term changes (due to apsidal motion for example), starspot activity, and quarter-to-quarter blending of the target flux with that from stars with small angular separations. Finally the phase offset parameter is multiplied by P to find the time of eclipse. Our measurements appear in Table 2 (given in full as a machine readable table in the electronic version) that lists the target KIC number, a 1 or 2 for primary (deeper) or secondary eclipse, the eclipse time T_E and its uncertainty, and the depth scaling parameter D_E and its uncertainty. A comparison of our eclipse timing measurements with those from Conroy et al. (2014) and Zasche et al. (2015) shows excellent agreement, although there may be a small constant offset between the results due to differences in measurement techniques.

The eclipse times were then fit using a quadratic function for both the primary and secondary eclipses independently

$$T_E = T + PE + QE^2 \quad (2)$$

where E is the integer eclipse cycle number in the time series. The final parameter is related to the period derivative by

$$\dot{P}/P = 2Q/P^2. \quad (3)$$

We included the quadratic term QE^2 to search for long term trends related to mass transfer in interacting binaries and to orbital motion about a tertiary in a very long period orbit (Section 4). However, in cases where the time span of observations is similar to a tertiary orbital period (see KIC 04848423), the curve is more complicated than a simple parabola and the value of Q has no physical meaning. We treated the primary and secondary eclipse times independently in order to search for cases of non-zero orbital eccentricity (in which the intervals between primary and secondary eclipse may differ from half the period) and possible apsidal motion (causing differences in measured period; Otero 2003). Table 1 lists the fitting results in two rows per target for each of the primary and secondary eclipses (KIC number appended with a P or S, respectively). The columns of Table 1 give the KIC number, the average uncertainty in eclipse time measurement I (internal scatter), the standard deviation of the full set of measurements E (external scatter), the epoch of minimum T near the middle of the time series, the orbital period P , the period derivative \dot{P}/P , the standard deviation of the eclipse depth factor $\sigma(D_E)$, and a code to references on eclipse timings for the target. The numbers in parentheses give the uncertainties in terms of the last digit quoted. The

final column includes the code ECC to identify those systems with a non-zero eccentricity as indicated by significantly differing epochs of eclipse, $(|T(\text{sec}) - T(\text{pri}) - P/2| \bmod P) > 0$.

A graphical representation of the results is shown in Figure Set 1 (given in full in the electronic version). Each figure shows the net variation of eclipse timing ($O = \text{observed}$) after subtraction of the linear trend ($C = T + PE = \text{calculated}$). In several cases the *Kepler* measurements are augmented with timings from before and after *Kepler* from Zasche et al. (2015) (see §3). The plots appear often as scatter diagrams with no trends visible in either the primary or secondary eclipse measurements (for example, KIC 5738698; Fig. 1.16). However, trends do appear in many cases that are related to starspots, apsidal motion (KIC 04544587; Fig. 1.6; Hambleton et al. 2013), long term period changes, or the light time changes associated with orbital motion about a third star. We focus on the latter group in the next section.

The variations due to starspots are often found only in the timings for the eclipse of the cooler secondary component (for example, KIC 10581918 = WX Dra, an Algol-type binary; Fig. 1.35). These variations are caused by the change in the surface intensity and center of light over the visible hemisphere (Kalimeris et al. 2002; Tran et al. 2013). For example, suppose a dark spot group rotates into view on the approaching portion of the eclipsed star. This will cause the overall flux to drop around the time of eclipse, and the eclipse minimum will occur slightly later as the transiting star passes over the center of light on the receding (brighter) portion of the visible hemisphere. Orosz et al. (2012) and Holczer et al. (2015) have documented how the starspot illumination changes lead to a general anticorrelation between the local flux derivative and eclipse time deviation, and this trend is found for example in the eclipse light curve of KIC 10581918 (see Fig. 1.35 of Gies et al. 2012). We suspect that most of the cases that show “random-walk” kinds of variations on relatively short time scales are due to starspot activity on one or both components.

Finally we note that the $O - C$ diagram for the eccentric binary KIC 04544587 (Fig. 1.6) looks quite different from what appeared in our earlier work (Fig. 2.6 of Gies et al. 2012) because we now determine separate periods for the primary and secondary eclipse times so that the differing slopes in the earlier figure are absent here.

3. Preliminary Orbital Solutions

The light time effect variations due to a third star may be difficult to detect if the third star’s orbital period is longer than the duration of the *Kepler* time series (4 years). In such cases, we may only sample a section of the linear or curved parts of the $O - C$

variation, so a full orbital fit must await further eclipse observations. On the other hand, the $O - C$ variations from shorter period companions may be sufficient for a preliminary orbital solution. We selected seven potential targets for orbital fits (listed in Table 3) from those that showed two inflection points in their $O - C$ changes in measurements for both the primary and secondary eclipses. There are supplementary timing measurements from Zasche et al. (2015) for five of these seven candidate systems, and we included these other timings in our orbital fits. However, because our eclipse fitting method differs from that adopted by Zasche et al., we first compared our eclipse times with theirs for the same *Kepler* observations to find a small mean difference ΔT (mean of T_E from this work minus that from Zasche et al.) that was added to the supplementary data. These small offsets are listed in column 11 of Table 3. The $O - C$ diagrams in Figure Set 1 include these supplementary timings for the five targets discussed by Zasche et al. (2015).

We fit the eclipse timings using a linear plus Keplerian model (Irwin 1952, 1959; Mayer 1990; Pribulla et al. 2005):

$$T_E = T_1 + PE + \frac{A}{\sqrt{1 - e^2 \cos^2 \omega}} \left[\frac{1 - e^2}{1 + e \cos \nu} \sin(\nu + \omega) + e \sin \omega \right] \quad (4)$$

where the semiamplitude is $A = (a_{12} \sin i) \sqrt{1 - e^2 \cos^2 \omega} / c$, a_{12} is the semimajor axis of the binary in its orbit around the common center of mass of the triple system, i is the inclination, e is the eccentricity, ω is the longitude of periastron, and ν is the true anomaly of the binary in its orbit about the center of mass of the triple system. The parameter ν is found from the outer orbit epoch of periastron T_3 , period P_3 , e , and time of eclipse. Note that we are ignoring physical perturbations of the inner orbit, because their associated amplitudes tend to be much lower than those of the light travel time effect for longer period orbits of the third star like those we are considering here (Gies et al. 2012; Rappaport et al. 2013). We made fits of the primary eclipse timings using the model formulation above and the MPFIT solver for parameters T_1 , P , A , e , ω , P_3 , and T_3 . For completeness, we then fit the secondary eclipse times with all these parameters fixed except the epoch T_2 . Our final results are listed in Table 3 together with a mass function for the third star (Frieboes-Conde & Herczeg 1973; Mayer 1990),

$$f(m_3) = \frac{(m_3 \sin i)^3}{(m_1 + m_2 + m_3)^2} = \frac{1}{P_3^2} \left[\frac{173.15 A}{\sqrt{1 - e^2 \cos^2 \omega}} \right]^3 \quad (5)$$

where A is given in units of days and P_3 in units of years. Again numbers in parentheses give the uncertainty in the last quoted digit that were taken as the maximum of the estimated errors from MPFIT and the absolute differences of results from trials made with some parameters fixed. We caution that these formal uncertainties are probably underestimates because the observations only record about one orbital cycle.

The derived orbital fits are shown as solid lines in Figure Set 1 for these seven candidate triples. The fits are satisfactory in every case, and the solutions are often driven by measurements made beyond the time span of the *Kepler* observations. Zasche et al. (2015) discuss the solutions for five of these triples, and in general our results agree within the uncertainties. Orbits for the other two, KIC 04574310 and KIC 04848423, are shown here for the first time.

4. Discussion

Our analysis of the eclipse timing variations has led to the identification of seven probable triples among our sample of 41 targets. Although this is a small sample, the detection rate of triples by the light travel time effect is $7/41 = 17\%$, which is consistent with estimates from other larger samples of *Kepler* eclipsing binaries (Rappaport et al. 2013; Conroy et al. 2014; Orosz 2015). The observed semiamplitudes range from 29 seconds for KIC 4574310 to 26 minutes for KIC 02305372. The associated mass functions generally indicate that the companions are probably lower mass, K-type stars (with the exception of KIC 04574310, which has a low mass function more consistent with a brown dwarf companion), but we caution that such mass estimates are lower limits because of the $\sin i$ factor in the mass function (equation 5). We might have detected even smaller semiamplitudes in principle, because there are a number of cases where the standard deviation of the timings is less than 10 seconds (see the external scatter E in column 3 of Table 1). Note that the inner binary periods are generally 5 days or less (with the exception of KIC 12071006 with $P = 6.096$ days), and planets orbiting eclipsing binaries have only been detected in systems with periods in excess of 7 days (Welsh et al. 2014). This may indicate that Kozai modulations with a third star have tended to clear away lower mass components in binaries with short orbital periods (Martin et al. 2015; Muñoz & Lai 2015).

It is certainly possible that other systems in our sample have distant third stars that have orbits longer than 4 years, in which we record only a small piece of the total $O - C$ variation. For example, there are seven systems with very large and similar parabolic variations observed in both the primary and secondary eclipses (KIC 03241619, KIC 03440230, KIC 04851217, KIC 05621294, KIC 06206751, KIC 09602595, KIC 10736223; see Table 1). These systems may represent those that were recorded during wide orbit phases of rapid change. If we imagine that the orbital $O - C$ variations are approximately sinusoidal, then during the *Kepler* window of observations we might expect about half to be found in the nearly linear part (undetected in the $O - C$ variations) and the other half to be found in curved portions (yielding a significant \dot{P}/P variation). The latter group would have equal

numbers of positive and negative values of period derivative, and indeed we find nearly equal numbers (three positive and four negative) among those cases with large parabolic variations. Similar numbers of positive and negative valued quadratic changes in $O - C$ were also found among eclipsing binaries in the SuperWASP survey (Lohr et al. 2015), consistent with the idea that many of these are triples with incompletely covered, long orbits. We caution that some of the weaker parabolic trends may result from long term variations in starspot activity and not orbital motion (for example, the case of KIC 02708156 in Fig. 1.2). These cases may often be identified by correlated variations between $O - C$ and the eclipse depth scaling parameter D_E .

Our analysis of the eclipse timing measurements has provided us with a reliable set of orbital ephemerides and a list of probable triples among this sample of eclipsing binaries. In future papers, we will use these results in combined spectroscopic and photometric analyses to determine the stellar properties, evolutionary state, and pulsational characteristics. We plan to investigate the influence of “third light” components on the interpretation of the orbital light curve and to search for direct evidence of the spectral lines of tertiaries among the triple star candidates.

Kepler was competitively selected as the tenth Discovery mission. Funding for this mission is provided by NASA’s Science Mission Directorate. This study was supported by NASA grants NNX12AC81G, NNX13AC21G, and NNX13AC20G. This material is based upon work supported by the National Science Foundation under Grant No. AST-1411654. Institutional support has been provided from the GSU College of Arts and Sciences and from the Research Program Enhancement fund of the Board of Regents of the University System of Georgia, administered through the GSU Office of the Vice President for Research and Economic Development. All of the data presented in this paper were obtained from the Mikulski Archive for Space Telescopes (MAST). STScI is operated by the Association of Universities for Research in Astronomy, Inc., under NASA contract NAS5-26555. Support for MAST for non-HST data is provided by the NASA Office of Space Science via grant NNX09AF08G and by other grants and contracts.

Facilities: Kepler

REFERENCES

- Armstrong, D., Pollacco, D., Watson, C. A., et al. 2012, *A&A*, 545, L4
 Armstrong, D. J., Kirk, J., Lam, K. W. F., et al. 2015, *A&A*, 579, A19

- Borkovits, T., Rappaport, S., Hajdu, T., & Sztakovics, J. 2015, *MNRAS*, 448, 946
- Borkovits, T., Derekas, A., Kiss, L. L., et al. 2013, *MNRAS*, 428, 1656
- Carter, J. A., Fabrycky, D. C., Ragozzine, D., et al. 2011, *Science*, 331, 562
- Conroy, K. E., Prša, A., Stassun, K. G., et al. 2014, *AJ*, 147, 45
- Derekas, A., Kiss, L. L., Borkovits, T., et al. 2011, *Science*, 332, 216
- Duchêne, G., & Kraus, A. 2013, *ARA&A*, 51, 269
- Frieboes-Conde, H., & Herczeg, T. 1973, *A&AS*, 12, 1
- Gies, D. R., Williams, S. J., Matson, R. A., et al. 2012, *AJ*, 143, 137
- Hambleton, K. M., Kurtz, D. W., Prša, A., et al. 2013, *MNRAS*, 434, 925
- Holczer, T., Shporer, A., Mazeh, T., et al. 2015, *ApJ*, 807, 170
- Irwin, J. B. 1952, *ApJ*, 116, 211
- . 1959, *AJ*, 64, 149
- Kalimeris, A., Rovithis-Livaniou, H., & Rovithis, P. 2002, *A&A*, 387, 969
- LaCourse, D. M., Jek, K. J., Jacobs, T. L., et al. 2015, *MNRAS*, 452, 3561
- Lee, J. W., Hong, K., & Hinse, T. C. 2015, *AJ*, 149, 93
- Lohr, M. E., Norton, A. J., Payne, S. G., West, R. G., & Wheatley, P. J. 2015, *A&A*, 578, A136
- Markwardt, C. B. 2009, in *Astronomical Society of the Pacific Conference Series*, Vol. 411, *Astronomical Data Analysis Software and Systems XVIII*, ed. D. A. Bohlender, D. Durand, & P. Dowler, 251
- Martin, D. V., Mazeh, T., & Fabrycky, D. C. 2015, *MNRAS*, 453, 3554
- Mayer, P. 1990, *Bulletin of the Astronomical Institutes of Czechoslovakia*, 41, 231
- Muñoz, D. J., & Lai, D. 2015, *Proceedings of the National Academy of Science*, 112, 9264
- Naoz, S., & Fabrycky, D. C. 2014, *ApJ*, 793, 137
- Orosz, J. A. 2015, *ArXiv e-prints*, 1503.07295

- Orosz, J. A., Welsh, W. F., Carter, J. A., et al. 2012, *Science*, 337, 1511
- Otero, S. A. 2003, *Information Bulletin on Variable Stars*, 5482, 1
- Pribulla, T., Chochol, D., Tremko, J., & Kreiner, J. M. 2005, in *Astronomical Society of the Pacific Conference Series*, Vol. 335, *The Light-Time Effect in Astrophysics: Causes and cures of the O-C diagram*, ed. C. Sterken, 103
- Prša, A., Batalha, N., Slawson, R. W., et al. 2011, *AJ*, 141, 83
- Rappaport, S., Deck, K., Levine, A., et al. 2013, *ApJ*, 768, 33
- Slawson, R. W., Prša, A., Welsh, W. F., et al. 2011, *AJ*, 142, 160
- Tokovinin, A., Thomas, S., Sterzik, M., & Udry, S. 2006, *A&A*, 450, 681
- Tran, K., Levine, A., Rappaport, S., et al. 2013, *ApJ*, 774, 81
- Welsh, W. F., Orosz, J. A., Carter, J. A., & Fabrycky, D. C. 2014, in *IAU Symposium*, Vol. 293, *Formation, Detection, and Characterization of Extrasolar Habitable Planets*, ed. N. Haghighipour, 125
- Zasche, P., Wolf, M., Kučáková, H., et al. 2015, *AJ*, 149, 197

Table 1. Eclipsing Binary Properties

KIC	I (sec)	E (sec)	T (BJD-2,400,000)	P (day)	\dot{P}/P (10^{-6} year $^{-1}$)	$\sigma(D_E)$	References ^a
02305372P	25.3	178.1	55693.58496 (2)	1.40469191 (3)	9.63 (4)	0.018	C14, Z15
02305372S	35.0	222.3	55701.31436 (5)	1.4046910 (2)	11.4 (2)	0.038	...
02708156P	21.2	51.8	55690.03950 (2)	1.89126793 (6)	-1.91 (6)	0.008	C14
02708156S	33.0	128.7	55692.87715 (5)	1.8912707 (2)	-0.07 (4)	0.033	...
03241619P	26.6	58.7	55694.50030 (2)	1.70334737 (8)	2.18 (9)	0.015	...
03241619S	25.5	50.5	55691.94541 (3)	1.70334676 (5)	2.09 (6)	0.041	...
03327980P	29.4	4.5	55699.074202 (3)	4.23102186 (3)	-0.021 (2)	0.002	...
03327980S	38.8	4.4	55688.494827 (3)	4.23102201 (3)	-0.013 (2)	0.002	...
03440230P	24.4	112.8	55690.39643 (2)	2.88110022 (9)	-5.87 (6)	0.004	C14, Z15
03440230S	33.8	135.8	55700.48186 (7)	2.8811004 (3)	-4.8 (2)	0.018	...
04544587P	24.9	13.9	55689.673044 (7)	2.18909811 (3)	0.45 (2)	0.006	H13, ECC
04544587S	27.3	13.7	55688.910266 (9)	2.18913048 (4)	-0.17 (1)	0.006	...
04574310P	18.4	20.1	55644.346499 (6)	1.30622004 (1)	0.80 (2)	0.003	C14
04574310S	12.0	22.6	55646.30602 (1)	1.30622004 (2)	0.45 (2)	0.007	...
04660997P	15.4	37.5	55654.43913 (1)	0.56256064 (2)	-0.50 (4)	0.024	C14
04660997S	25.7	53.2	55647.40777 (1)	0.56256075 (3)	-1.37 (5)	0.075	...
04665989P	22.4	1.8	55646.917282 (1)	2.248067587 (7)	0.0125 (7)	0.001	C14
04665989S	31.1	3.3	55648.041437 (2)	2.24806759 (1)	0.0064 (9)	0.002	...
04678873P	22.7	42.0	55364.39581 (3)	1.8788767 (2)	0.7 (1)	0.015	...
04678873S	130.1	357.6	55365.3373 (3)	1.878880 (2)	-16. (4)	0.171	...
04848423P	58.5	213.1	55928.7090 (1)	3.0036456 (8)	22.2 (8)	0.004	...
04848423S	59.0	215.4	55933.2150 (1)	3.0036465 (8)	22.0 (8)	0.004	...
04851217P	67.9	38.1	55643.10900 (1)	2.47028357 (5)	1.71 (4)	0.004	C14, ECC
04851217S	49.4	39.5	55649.23501 (1)	2.47028209 (5)	1.93 (3)	0.003	...
05444392P	16.8	24.1	55688.84830 (1)	1.51952885 (3)	0.054 (8)	0.018	C14, O15
05444392S	25.2	47.9	55689.60795 (2)	1.51952893 (7)	-0.06 (2)	0.019	...
05513861P	23.6	350.6	55625.52615 (3)	1.51020817 (6)	17.70 (7)	0.001	C14, O15
05513861S	25.6	349.8	55627.79154 (3)	1.51020833 (6)	17.74 (7)	0.001	...
05621294P	15.2	46.7	55693.432093 (6)	0.938904885 (9)	-2.40 (2)	0.004	C14, L15, Z15, ECC
05621294S	52.8	105.5	55690.14750 (3)	0.93890558 (5)	-3.80 (9)	0.021	...
05738698P	31.2	3.6	55692.334870 (2)	4.80877394 (3)	0.0062 (7)	0.002	...
05738698S	32.1	4.4	55680.314028 (3)	4.80877398 (4)	-0.040 (3)	0.002	...
06206751P	14.7	44.7	55683.783072 (8)	1.24534282 (3)	-1.36 (4)	0.018	C14
06206751S	23.6	73.9	55686.89665 (3)	1.24534280 (7)	-1.01 (9)	0.065	...
07368103P	85.4	28.9	55698.67906 (1)	2.18251565 (7)	-0.07 (2)	0.011	C14
07368103S	532.4	543.0	55697.5891 (3)	2.1825145 (9)	-1.3 (8)	0.075	...
08196180P	28.0	6.8	55695.751468 (5)	3.67166106 (4)	-0.024 (4)	0.004	ECC
08196180S	30.1	27.2	55686.21595 (2)	3.6716582 (1)	-0.07 (2)	0.017	...
08262223P	16.4	7.6	55692.217903 (3)	1.61301476 (1)	0.018 (3)	0.003	C14
08262223S	21.8	18.1	55689.798699 (7)	1.61301470 (3)	0.055 (8)	0.005	...
08552540P	16.8	33.0	55692.15027 (1)	1.06193424 (3)	-0.11 (1)	0.014	C14
08552540S	18.1	28.2	55690.55782 (1)	1.06193427 (2)	0.064 (8)	0.033	...
08553788P	14.8	147.2	55690.62207 (2)	1.60616355 (5)	-7.56 (6)	0.004	C14, O15, Z15
08553788S	26.9	144.9	55691.42530 (3)	1.60616375 (6)	-7.15 (8)	0.019	...
08823397P	19.3	2.2	55686.100164 (1)	1.506503703 (4)	-0.0052 (5)	0.001	C14

Table 1—Continued

KIC	I (sec)	E (sec)	T (BJD-2,400,000)	P (day)	\dot{P}/P (10^{-6} year $^{-1}$)	$\sigma(D_E)$	References ^a
08823397S	15.8	4.3	55694.386282 (2)	1.506503696 (6)	−0.0094 (6)	0.006	...
09159301P	26.5	18.1	55693.13726 (1)	3.04477179 (7)	0.22 (2)	0.003	C14
09159301S	174.7	92.5	55685.52674 (5)	3.0447725 (4)	0.0 (1)	0.020	...
09357275P	14.7	3.1	55643.386640 (1)	1.588298217 (5)	0.0239 (8)	0.002	C14
09357275S	16.7	14.5	55644.181081 (9)	1.58829821 (3)	−0.060 (7)	0.013	...
09402652P	11.0	192.0	55689.37059 (1)	1.07310425 (3)	−10.15 (4)	0.002	C14, Z15
09402652S	11.7	192.3	55692.05303 (1)	1.07310419 (3)	−10.12 (4)	0.002	...
09592855P	16.7	19.2	55691.664073 (7)	1.21932487 (2)	0.027 (4)	0.016	C14
09592855S	19.3	22.4	55692.273798 (7)	1.21932479 (2)	0.039 (6)	0.014	...
09602595P	19.3	75.7	55642.26003 (4)	3.5565108 (2)	−3.4 (1)	0.004	C14, ECC
09602595S	18.2	118.8	55633.3721 (1)	3.5565149 (5)	−5.1 (3)	0.029	...
09851944P	22.5	17.0	55646.150110 (9)	2.16390177 (5)	0.030 (6)	0.002	C14
09851944S	21.7	16.2	55634.248526 (8)	2.16390178 (4)	−0.06 (1)	0.003	...
09899416P	15.9	6.8	55689.965570 (2)	1.332564486 (7)	−0.048 (2)	0.005	C14, ECC
09899416S	9.8	25.8	55691.96413 (1)	1.33256397 (2)	0.99 (3)	0.006	...
10156064P	33.0	6.6	55648.858147 (5)	4.85593640 (6)	0.020 (2)	0.003	...
10156064S	21.5	5.8	55660.998491 (6)	4.85593649 (7)	0.025 (4)	0.003	...
10191056P	15.6	4.9	55688.135138 (3)	2.42749476 (2)	−0.0081 (9)	0.003	C14, ECC
10191056S	14.6	4.6	55684.495255 (2)	2.42749492 (1)	−0.035 (1)	0.004	...
10206340P	24.4	146.2	55710.0929 (1)	4.564401 (1)	3.1 (4)	0.011	C14
10206340S	33.3	176.1	55684.9895 (1)	4.564409 (1)	1.0 (4)	0.026	...
10486425P	34.9	93.4	55681.8090 (1)	5.2748191 (8)	1.8 (3)	0.053	...
10486425S	94.3	372.7	55705.5464 (2)	5.274817 (3)	0.1 (2)	0.157	...
10581918P	20.9	10.3	55744.790056 (4)	1.80186368 (2)	0.146 (7)	0.010	C14, Z15
10581918S	33.1	81.5	55754.70106 (4)	1.8018637 (2)	−0.4 (1)	0.039	...
10619109P	17.9	57.1	55642.31502 (2)	2.04516550 (8)	2.26 (6)	0.009	C14, ECC
10619109S	49.0	187.5	55647.4299 (1)	2.0451674 (5)	−1.2 (4)	0.050	...
10661783P	30.9	9.5	55692.541890 (4)	1.23136327 (1)	0.048 (3)	0.004	C14
10661783S	54.2	20.9	55691.926166 (7)	1.23136329 (2)	−0.038 (6)	0.006	...
10686876P	25.3	127.1	55632.12313 (1)	2.61841633 (5)	−6.50 (3)	0.009	Z15
10686876S	27.7	112.5	55646.52478 (2)	2.61841462 (8)	−5.88 (6)	0.027	...
10736223P	17.3	38.3	55692.697641 (3)	1.105094220 (6)	2.03 (1)	0.005	C14
10736223S	28.5	42.4	55695.46087 (1)	1.10509441 (2)	2.01 (4)	0.013	...
10858720P	11.4	12.3	55692.951773 (4)	0.952377626 (8)	0.0 (1)	0.004	C14
10858720S	12.4	6.2	55691.523165 (2)	0.952377609 (4)	−0.013 (1)	0.006	...
12071006P	38.5	55.2	55693.45930 (4)	6.0960295 (3)	−2.4 (1)	0.006	C14, ECC
12071006S	154.0	199.3	55696.5059 (2)	6.096043 (2)	3.5 (7)	0.024	...

^aC14 = Conroy et al. (2014); H13 = Hambleton et al. (2013); L15 = Lee et al. (2015); O15 = Orosz (2015); Z15 = Zasche et al. (2015); ECC = non-zero eccentricity.

Table 2. Eclipse Timing Measurements^a

KIC Number	Eclipse Type	T_E (BJD-2,400,000)	$\sigma(T_E)$ (day)	D_E	$\sigma(D_E)$
02305372	2	54965.26257	0.00052	0.993	0.007
02305372	1	54965.96121	0.00031	1.010	0.005
02305372	2	54966.66766	0.00054	0.993	0.007
02305372	1	54967.36578	0.00030	1.009	0.005
02305372	2	54968.07249	0.00054	0.996	0.008
02305372	1	54968.77050	0.00029	1.012	0.005
02305372	2	54969.47710	0.00054	0.992	0.008
02305372	1	54970.17523	0.00029	1.013	0.005
02305372	2	54970.88144	0.00053	0.996	0.007
02305372	1	54971.57993	0.00029	1.012	0.005
02305372	2	54972.28629	0.00050	0.994	0.007
02305372	1	54972.98458	0.00029	1.012	0.005

^aThe full table is available in the electronic version.

Table 3. Preliminary Orbital Elements

KIC Number	T_1 (BJD-2,450,000)	T_2 (BJD-2,450,000)	P (day)	A (day)	e	ω (deg)	P_3 (year)	T_3 (BJD-2,450,000)	$f(m_3)$ (M_\odot)	ΔT (day)	References ^a
02305372	5693.59615 (10)	5699.92166 (5)	1.4047174 (2)	0.018 (3)	0.59 (8)	106 (6)	11.338 (4)	4718 (100)	0.25 (12)	0.00186	Z15
04574310	5644.346644 (2)	5646.306053 (8)	1.306220105 (7)	0.000333 (10)	0.670 (20)	346 (5)	3.717 (38)	5937 (4)	0.000032 (3)	...	new
04848423	5928.710960 (21)	5933.217094 (27)	3.0036281 (11)	0.0047 (2)	0.29 (4)	210 (14)	2.81 (10)	6642 (19)	0.076 (11)	...	new
05513861	5624.02384 (2)	5629.30955 (9)	1.5102097 (2)	0.00826 (19)	0.12 (2)	7.4 (12)	6.06 (12)	6239 (13)	0.081 (6)	0.00070	C14, Z15
08553788	5690.61611 (4)	5691.419455 (19)	1.6061766 (8)	0.0073 (4)	0.720 (30)	238.2 (11)	8.6 (2)	6428 (6)	0.035 (5)	0.00083	Z15
09402652	5689.363683 (6)	5692.046455 (34)	1.07310717 (14)	0.00442 (3)	0.800 (3)	267.4 (5)	4.169 (21)	6346 (2)	0.0259 (6)	0.00015	Z15
10686876	5632.11773 (8)	5646.519555 (22)	2.6184131 (2)	0.0054 (5)	0.47 (10)	284 (2)	6.63 (7)	7016 (22)	0.019 (5)	-0.00060	Z15

^aC14 = Conroy et al. (2014); Z15 = Zasche et al. (2015); new = this paper.

Fig. Set 1. Eclipse timing variations

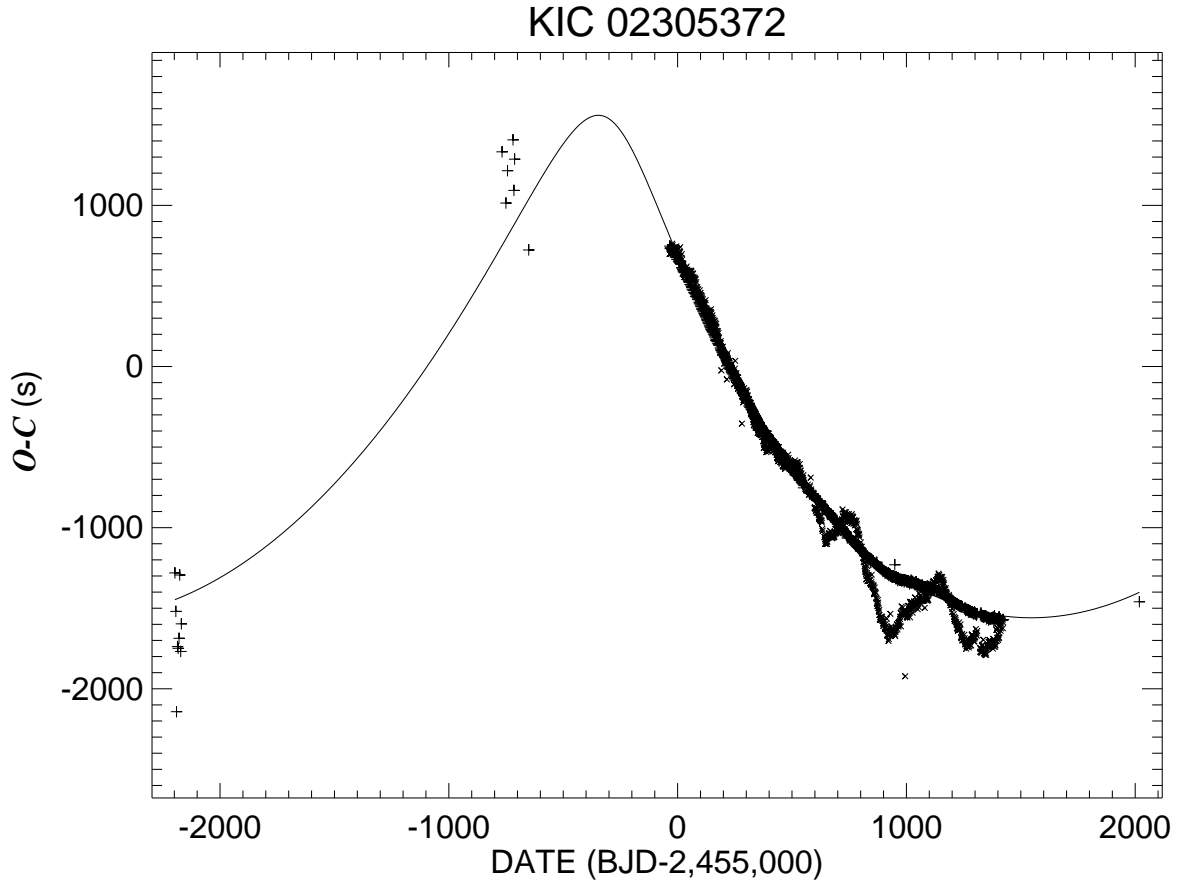


Fig. 1.1.— The observed minus calculated eclipse times relative to a linear ephemeris. The primary and secondary eclipse times are indicated by + and × symbols, respectively.

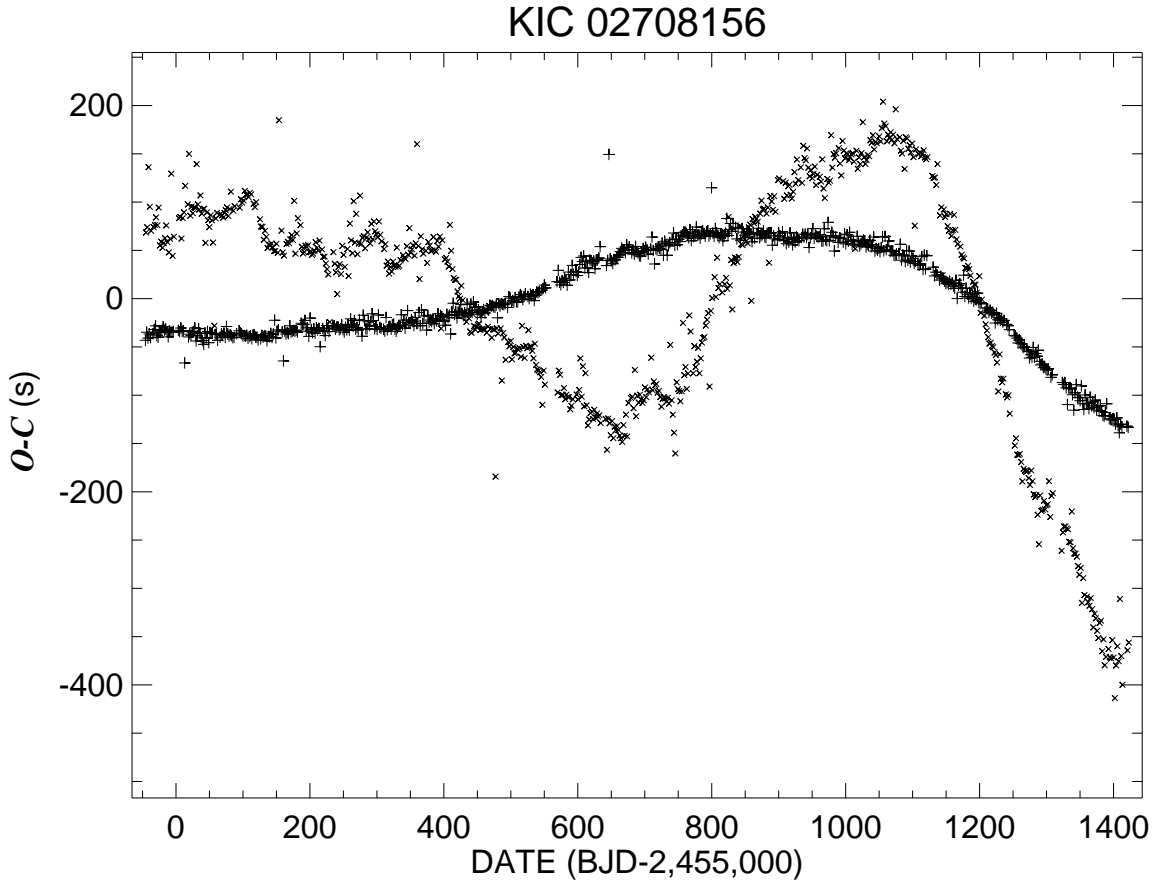


Fig. 1.2.— The observed minus calculated eclipse times relative to a linear ephemeris. The primary and secondary eclipse times are indicated by + and × symbols, respectively.

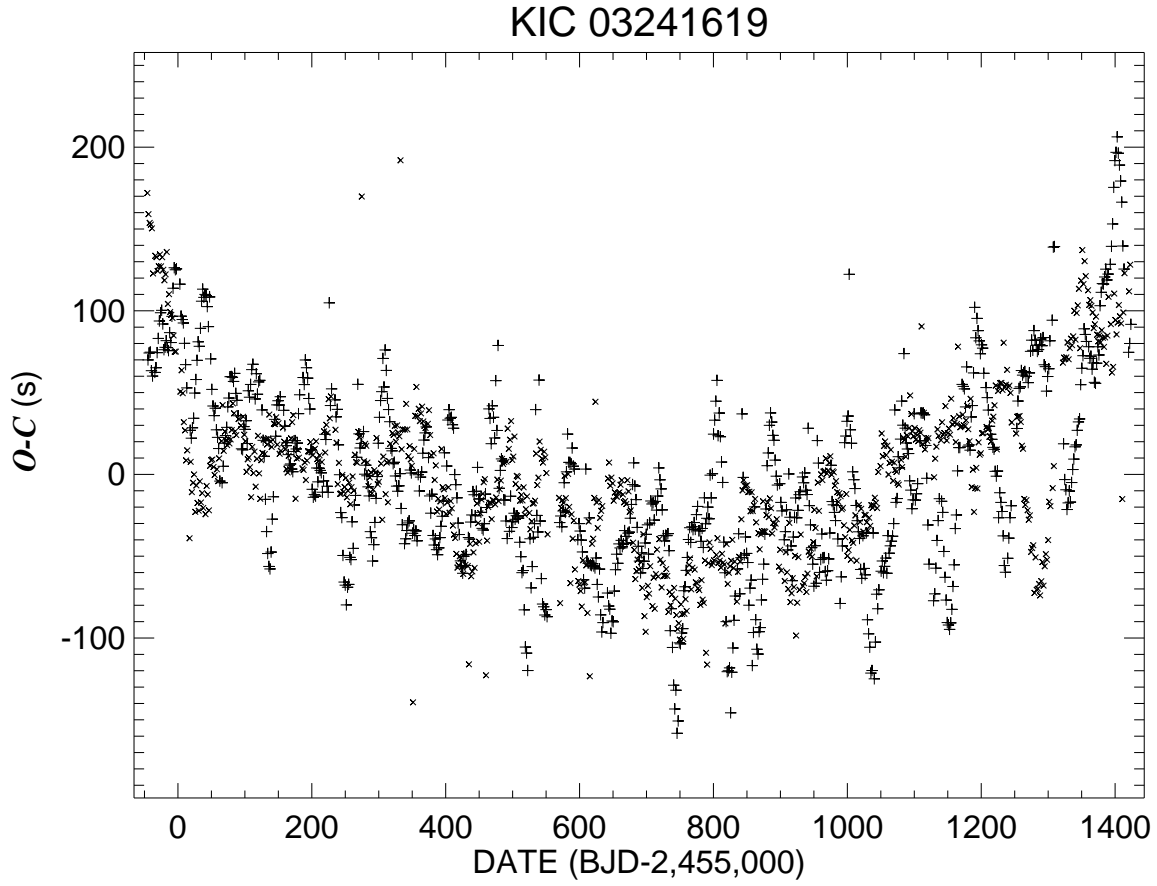


Fig. 1.3.— The observed minus calculated eclipse times relative to a linear ephemeris. The primary and secondary eclipse times are indicated by + and × symbols, respectively.

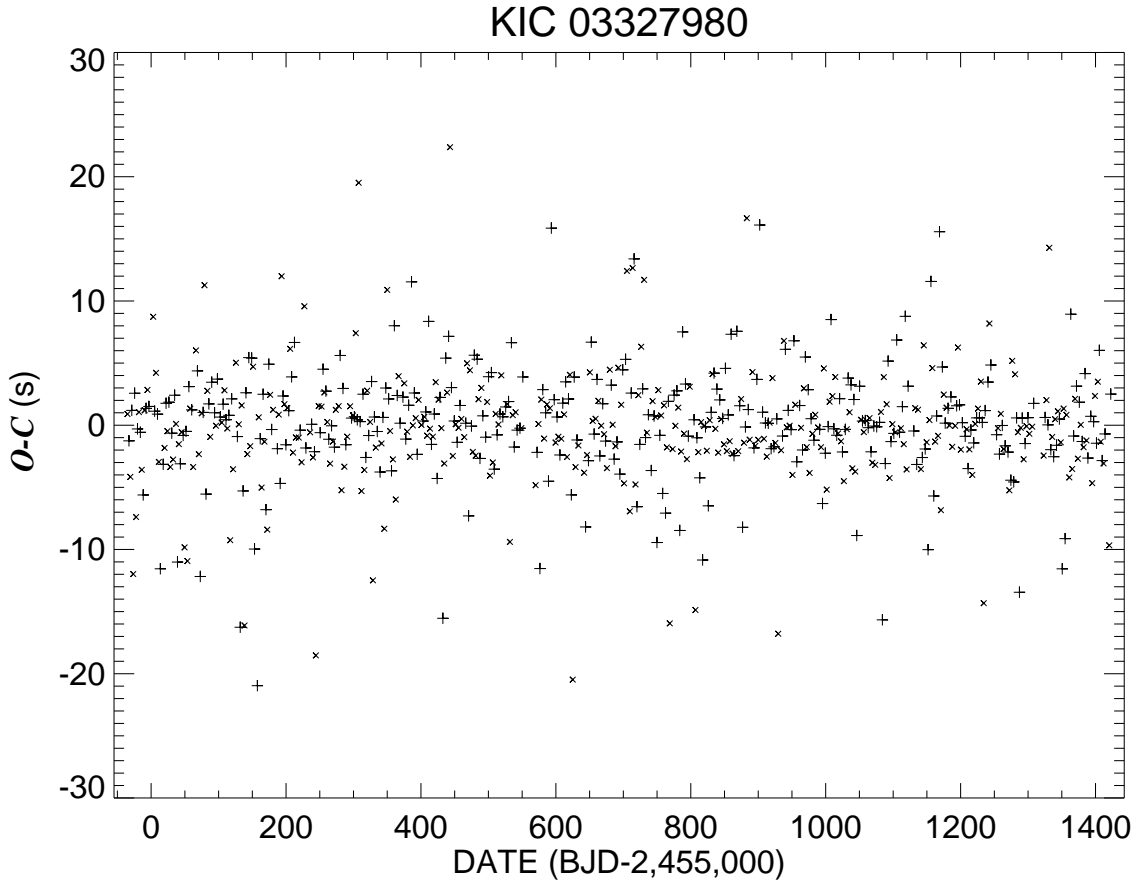


Fig. 1.4.— The observed minus calculated eclipse times relative to a linear ephemeris. The primary and secondary eclipse times are indicated by + and \times symbols, respectively.

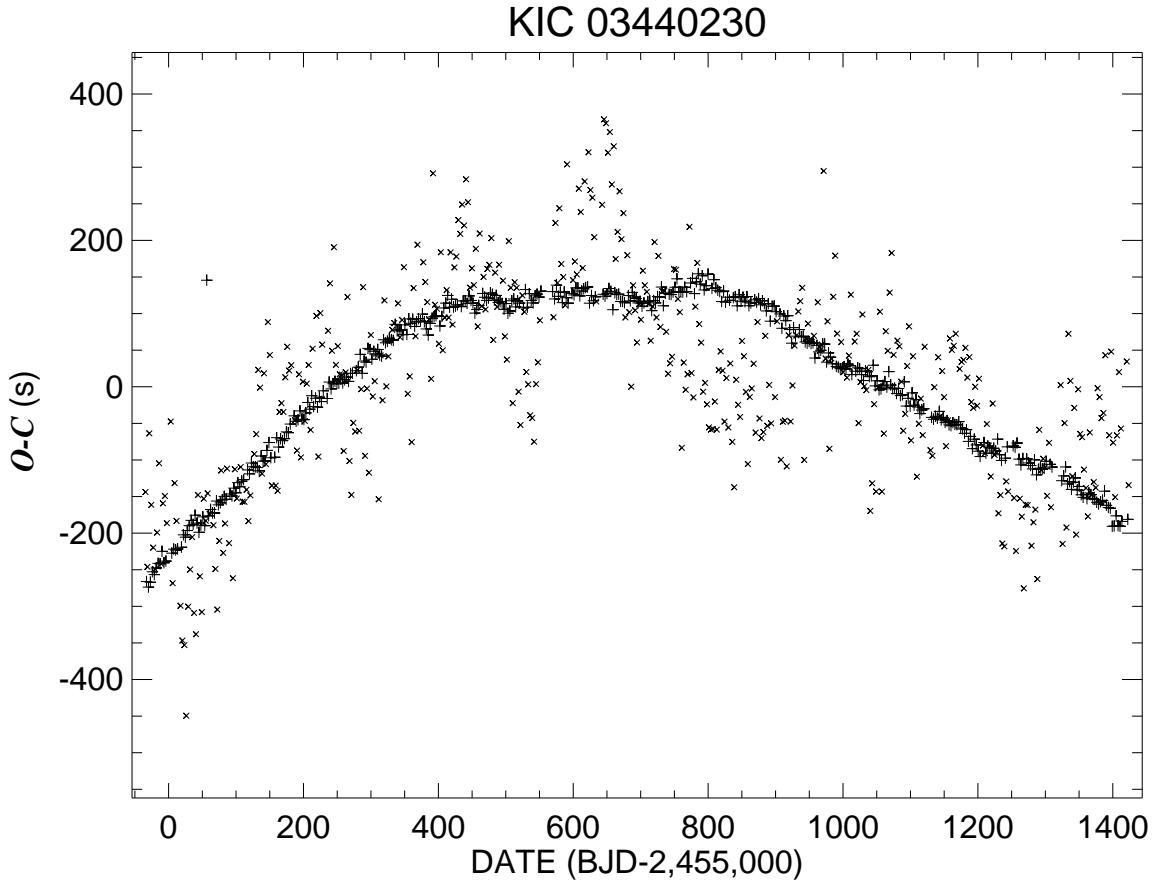


Fig. 1.5.— The observed minus calculated eclipse times relative to a linear ephemeris. The primary and secondary eclipse times are indicated by + and × symbols, respectively.

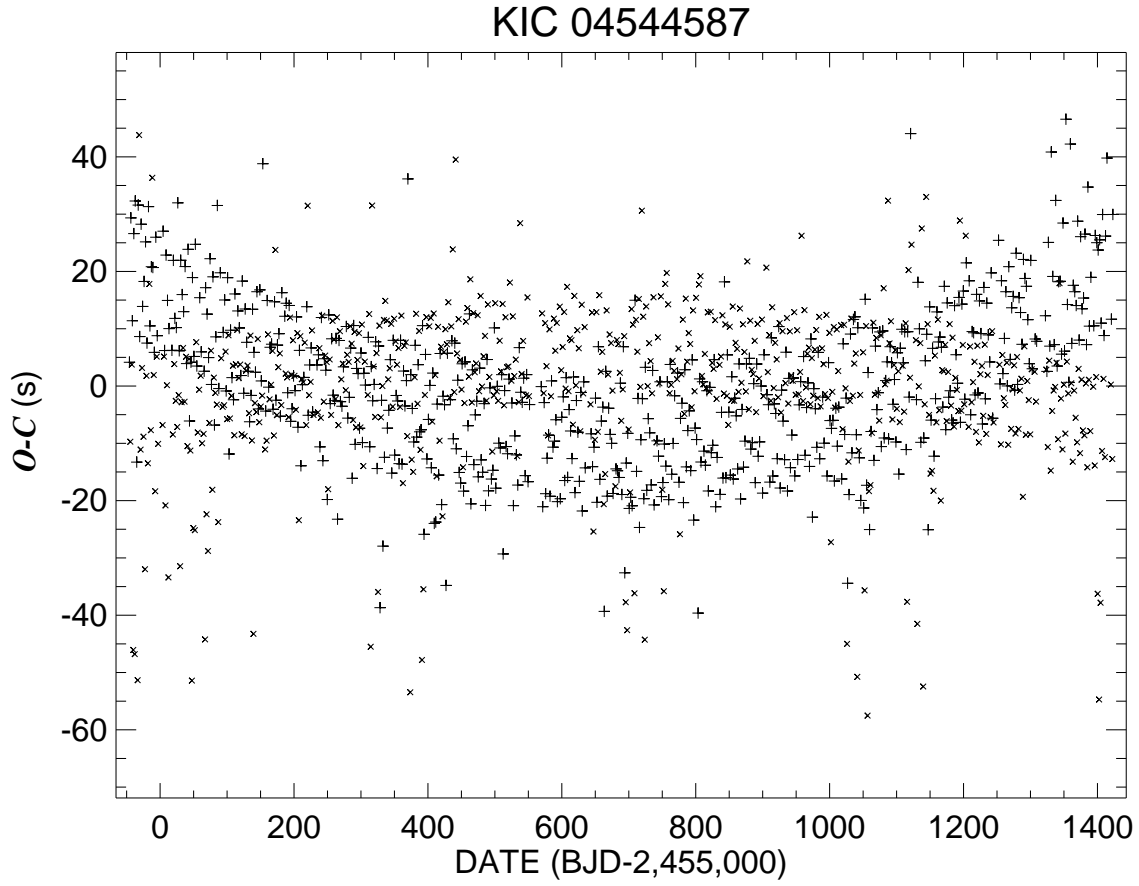


Fig. 1.6.— The observed minus calculated eclipse times relative to a linear ephemeris. The primary and secondary eclipse times are indicated by + and \times symbols, respectively.

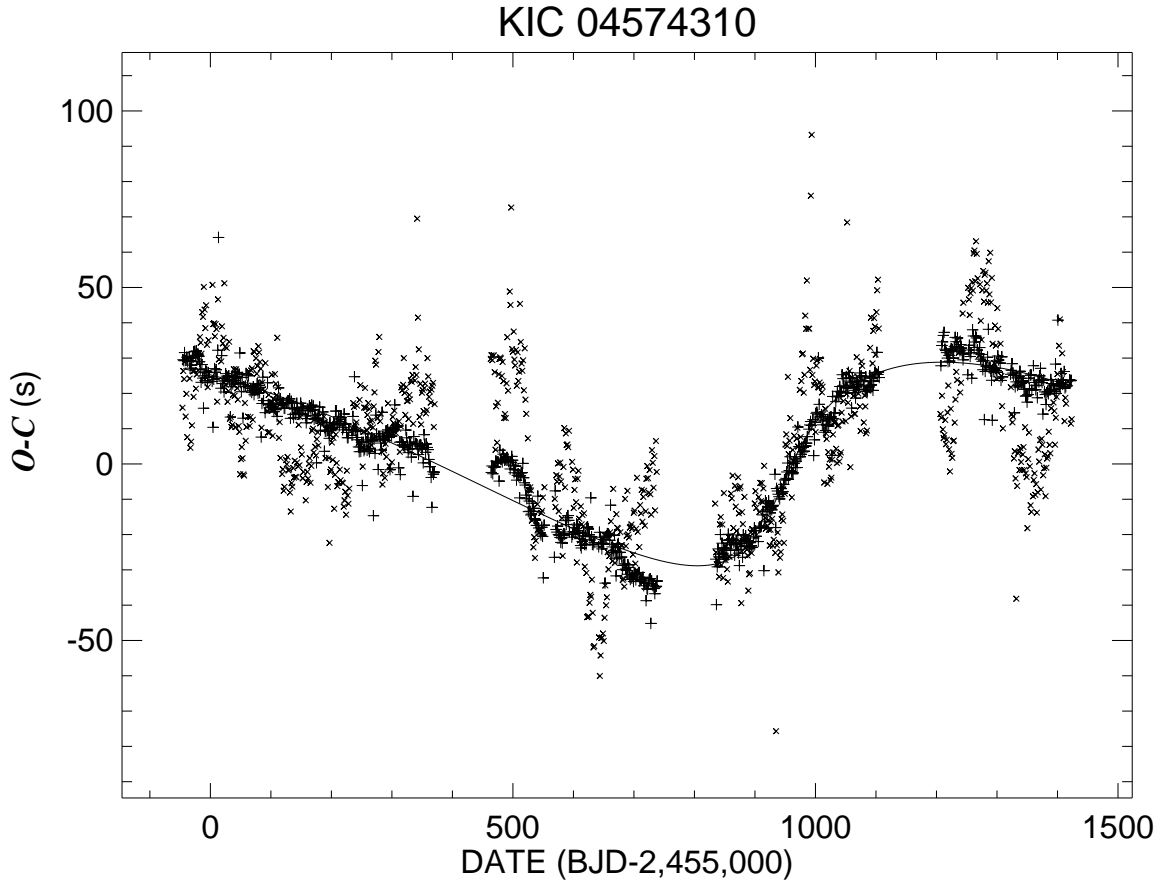


Fig. 1.7.— The observed minus calculated eclipse times relative to a linear ephemeris. The primary and secondary eclipse times are indicated by + and × symbols, respectively.

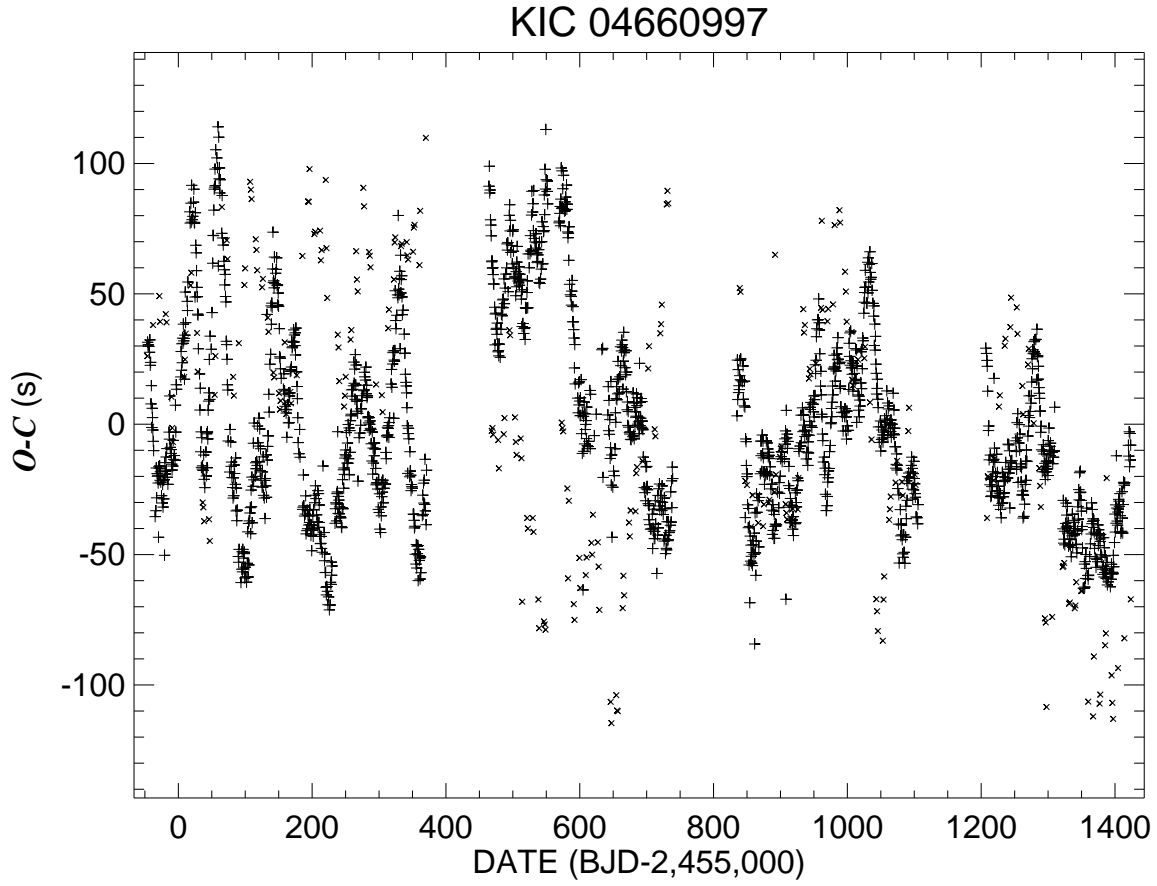


Fig. 1.8.— The observed minus calculated eclipse times relative to a linear ephemeris. The primary and secondary eclipse times are indicated by + and × symbols, respectively.

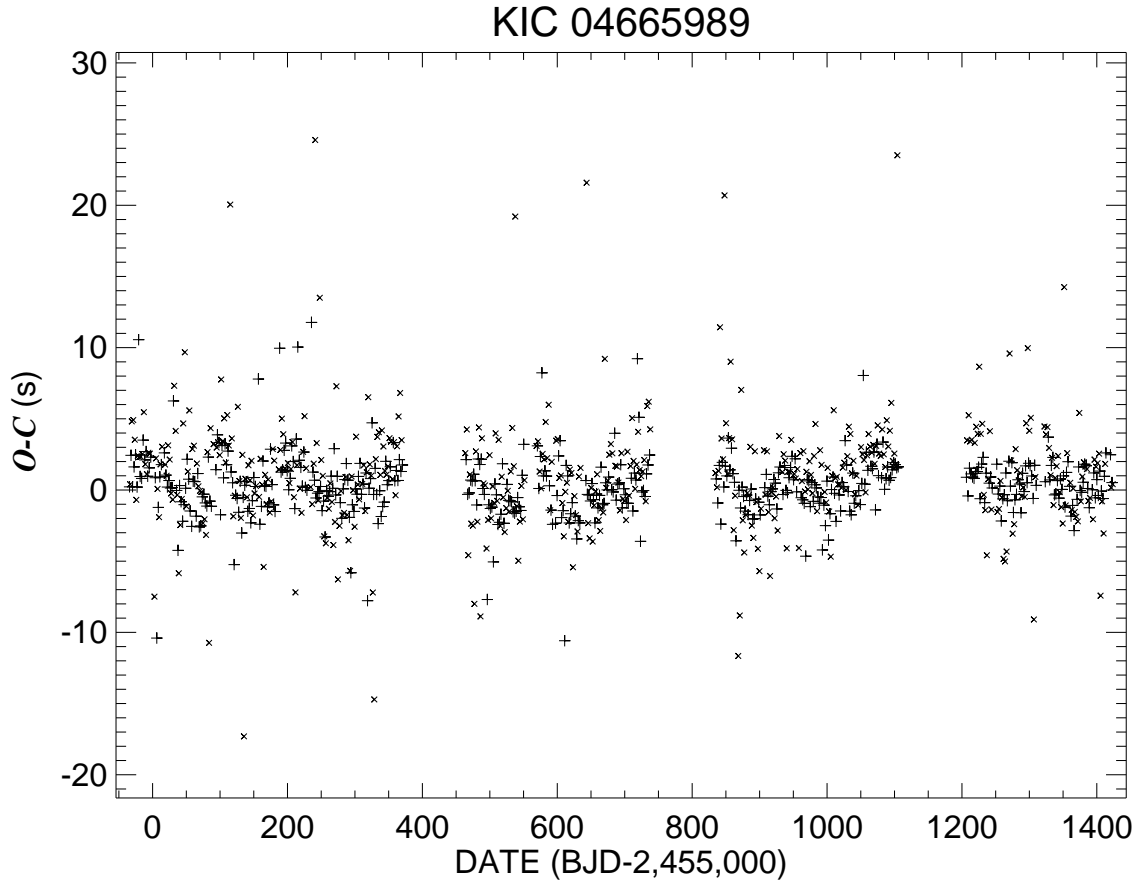


Fig. 1.9.— The observed minus calculated eclipse times relative to a linear ephemeris. The primary and secondary eclipse times are indicated by + and \times symbols, respectively.

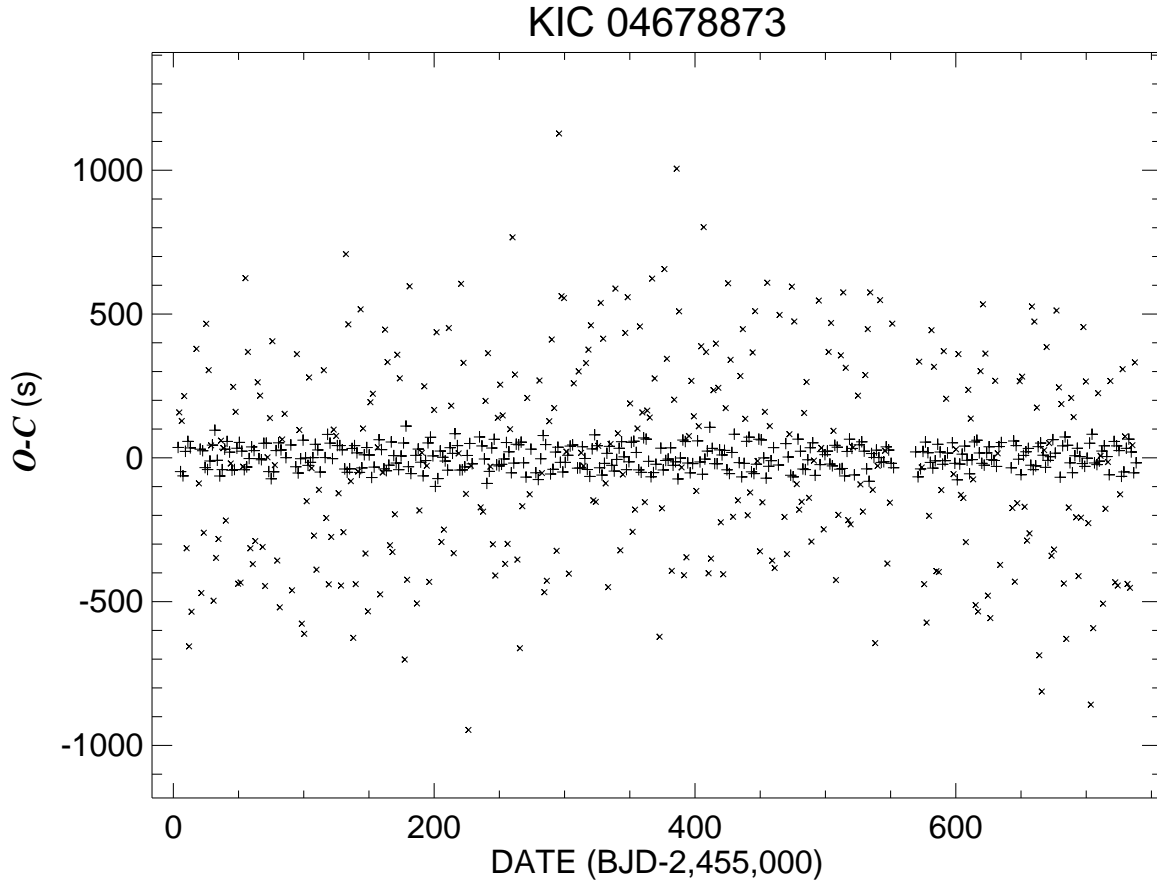


Fig. 1.10.— The observed minus calculated eclipse times relative to a linear ephemeris. The primary and secondary eclipse times are indicated by + and × symbols, respectively.

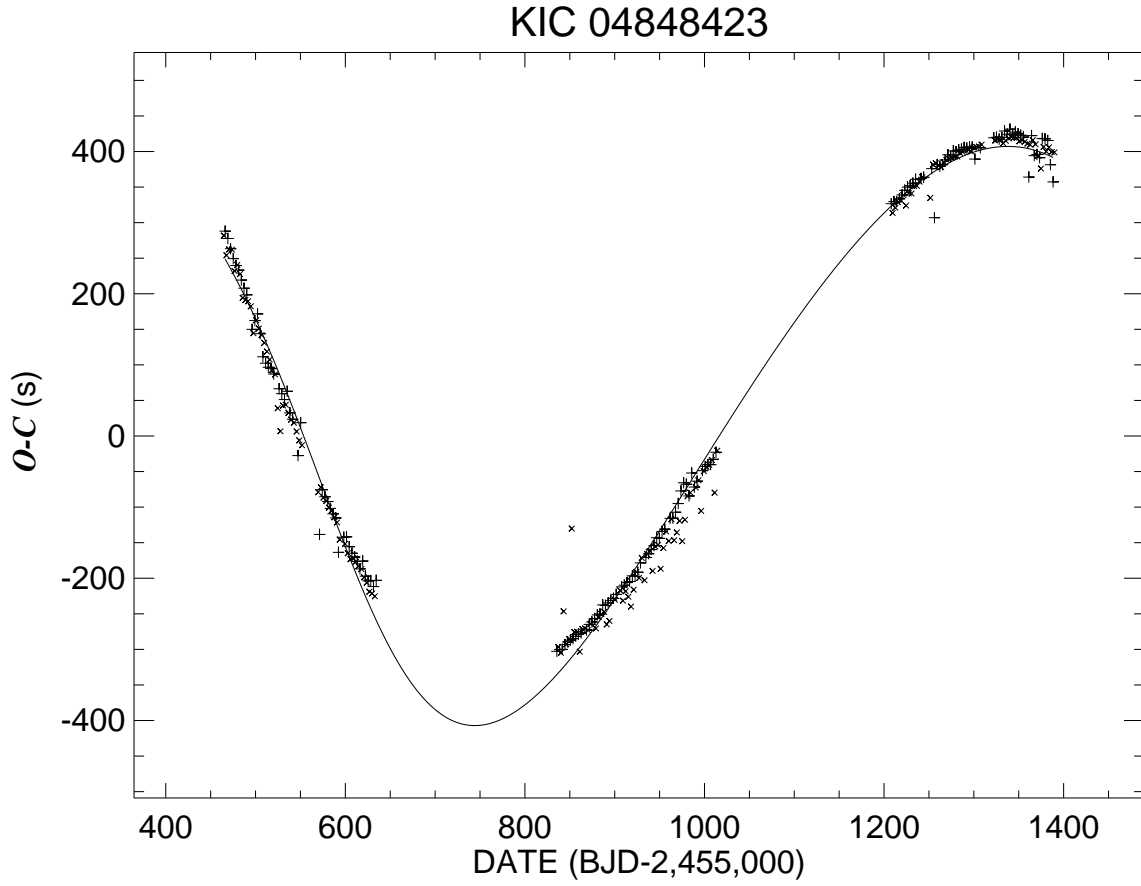


Fig. 1.11.— The observed minus calculated eclipse times relative to a linear ephemeris. The primary and secondary eclipse times are indicated by + and \times symbols, respectively.

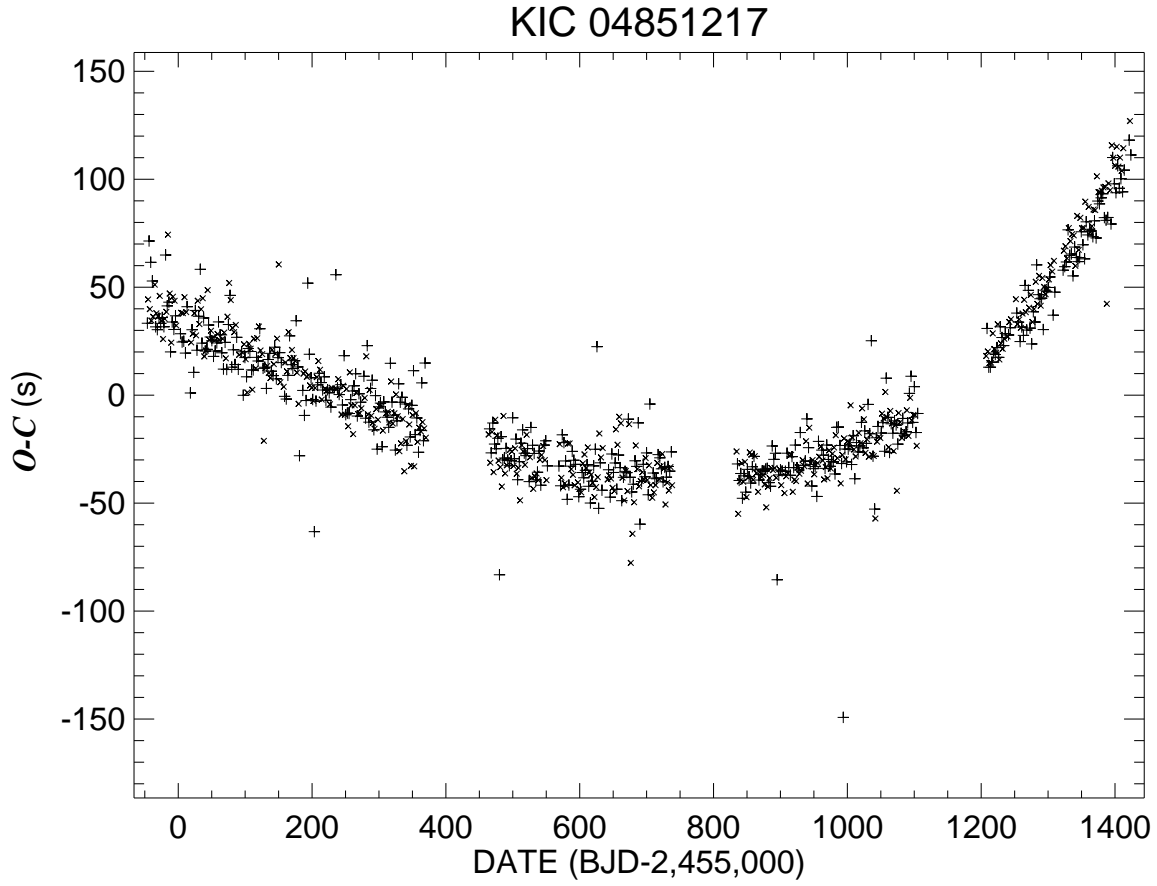


Fig. 1.12.— The observed minus calculated eclipse times relative to a linear ephemeris. The primary and secondary eclipse times are indicated by + and × symbols, respectively.

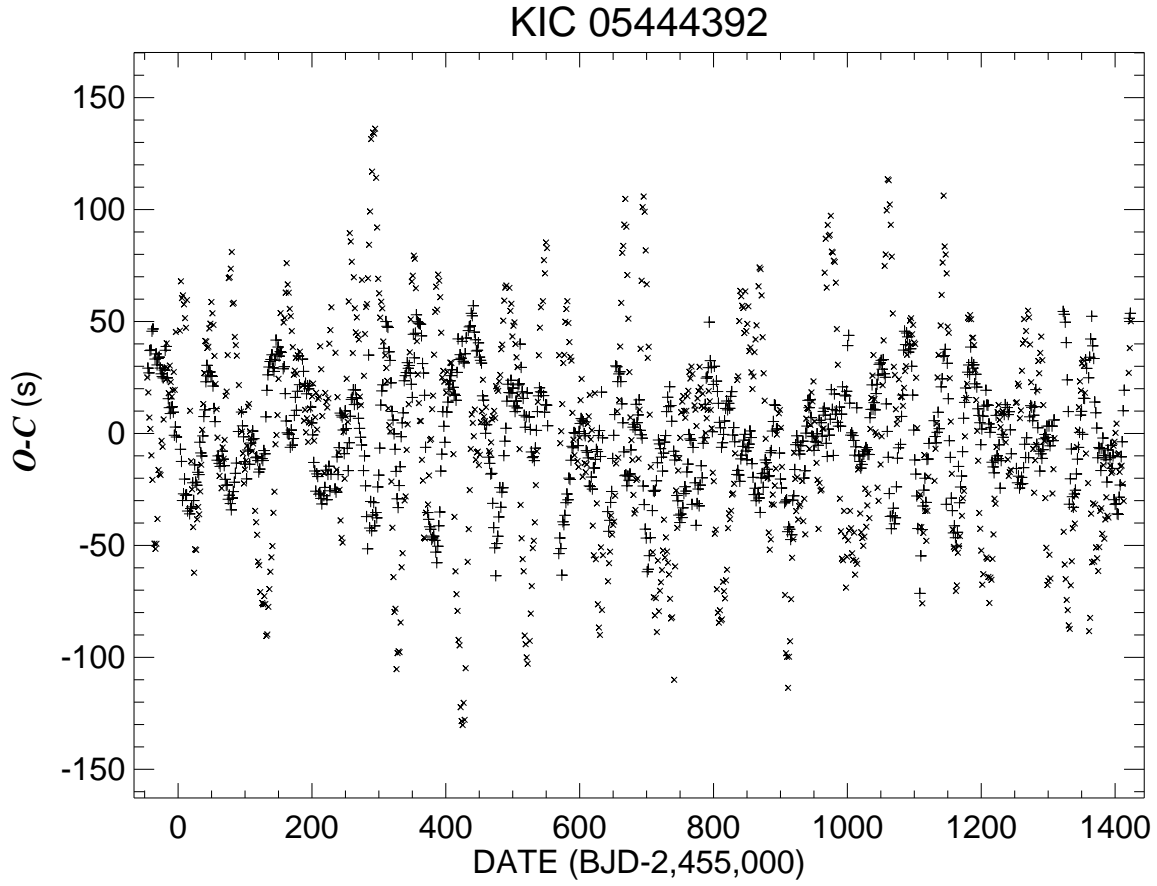


Fig. 1.13.— The observed minus calculated eclipse times relative to a linear ephemeris. The primary and secondary eclipse times are indicated by + and \times symbols, respectively.

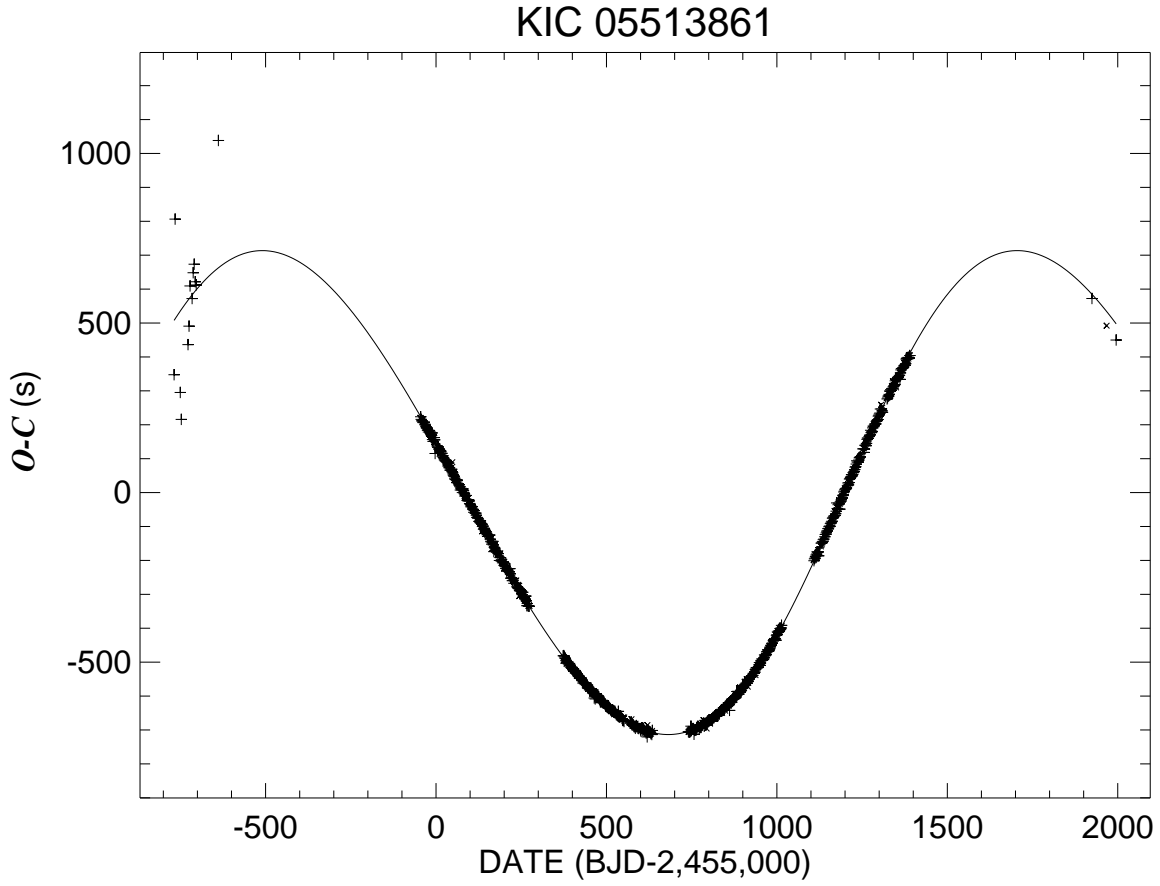


Fig. 1.14.— The observed minus calculated eclipse times relative to a linear ephemeris. The primary and secondary eclipse times are indicated by + and × symbols, respectively.

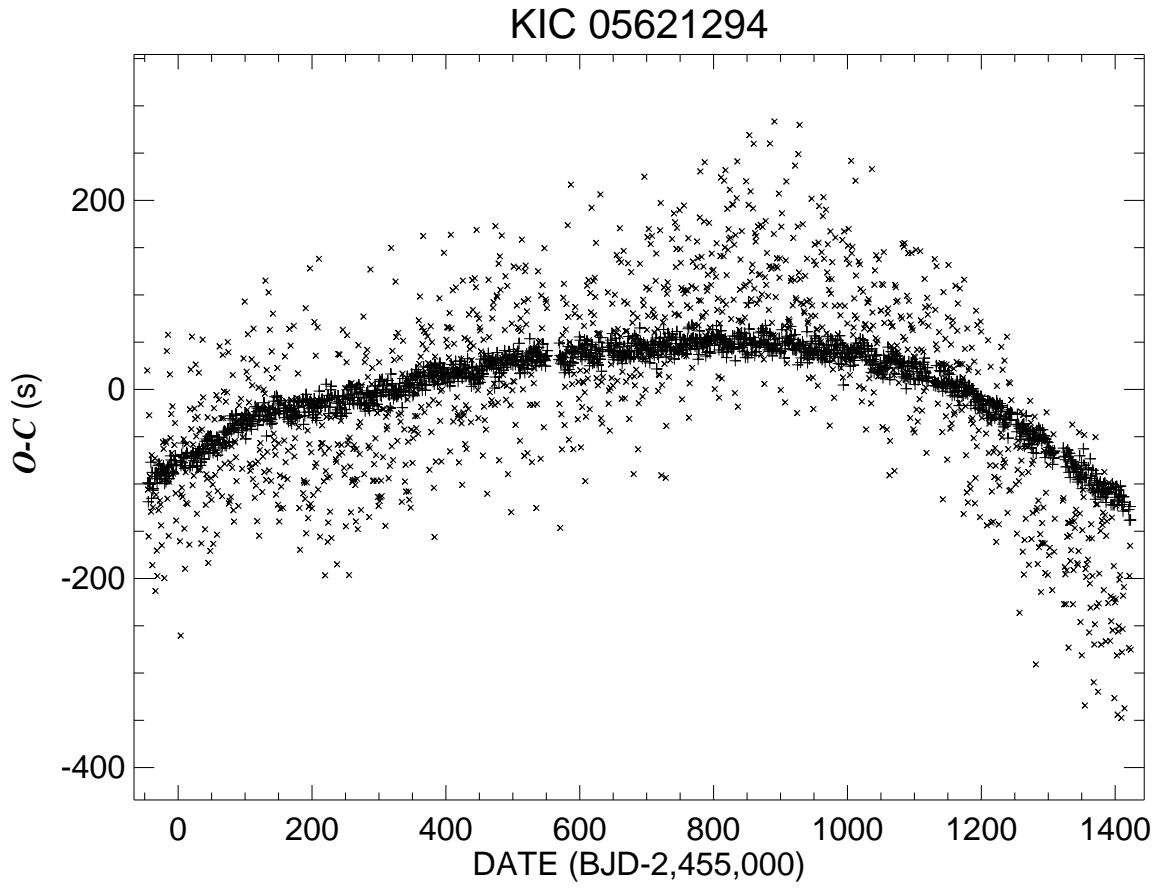


Fig. 1.15.— The observed minus calculated eclipse times relative to a linear ephemeris. The primary and secondary eclipse times are indicated by + and \times symbols, respectively.

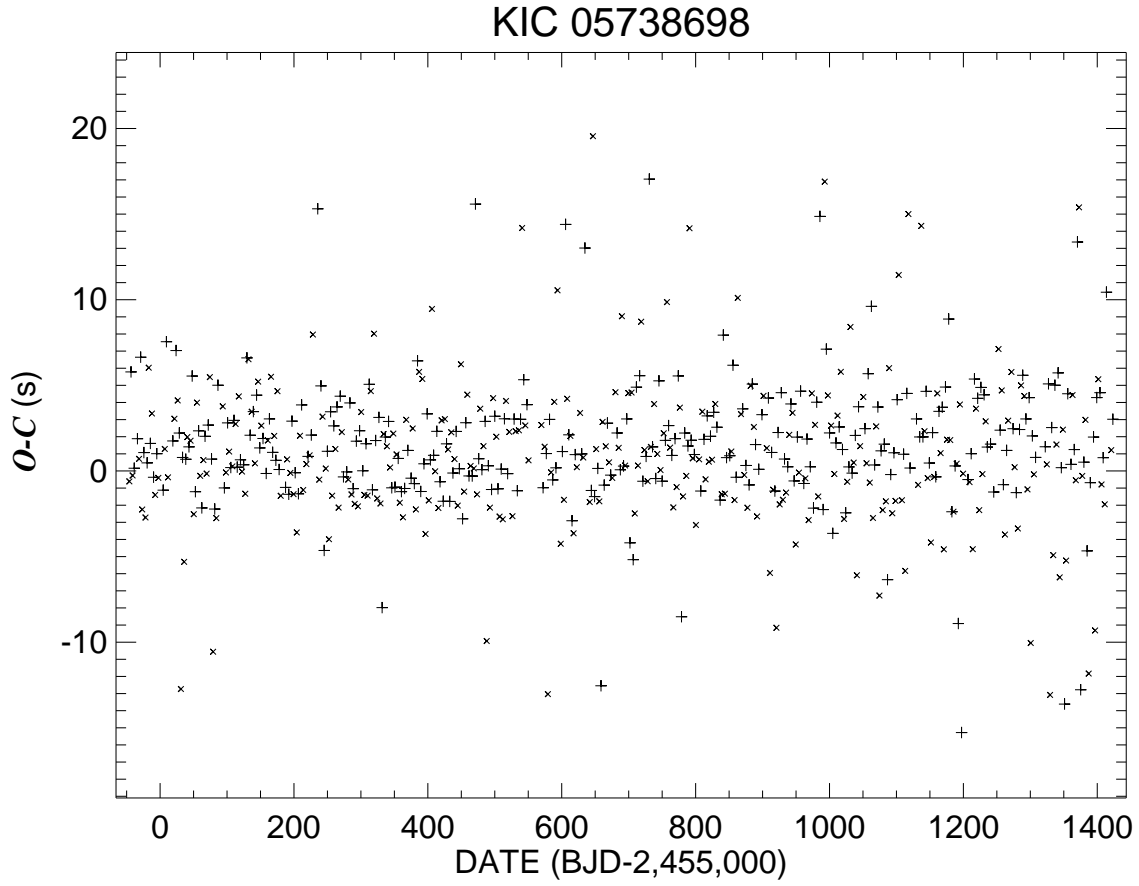


Fig. 1.16.— The observed minus calculated eclipse times relative to a linear ephemeris. The primary and secondary eclipse times are indicated by + and \times symbols, respectively.

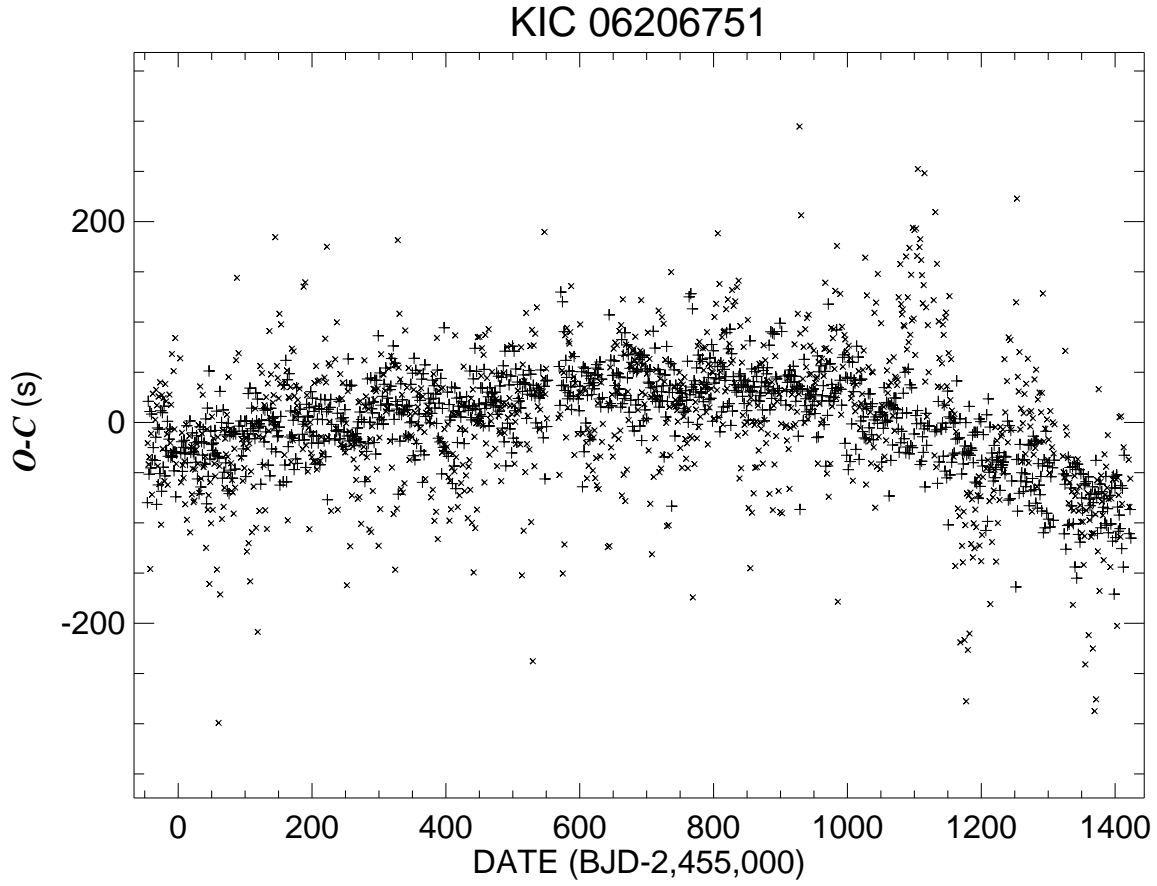


Fig. 1.17.— The observed minus calculated eclipse times relative to a linear ephemeris. The primary and secondary eclipse times are indicated by + and \times symbols, respectively.

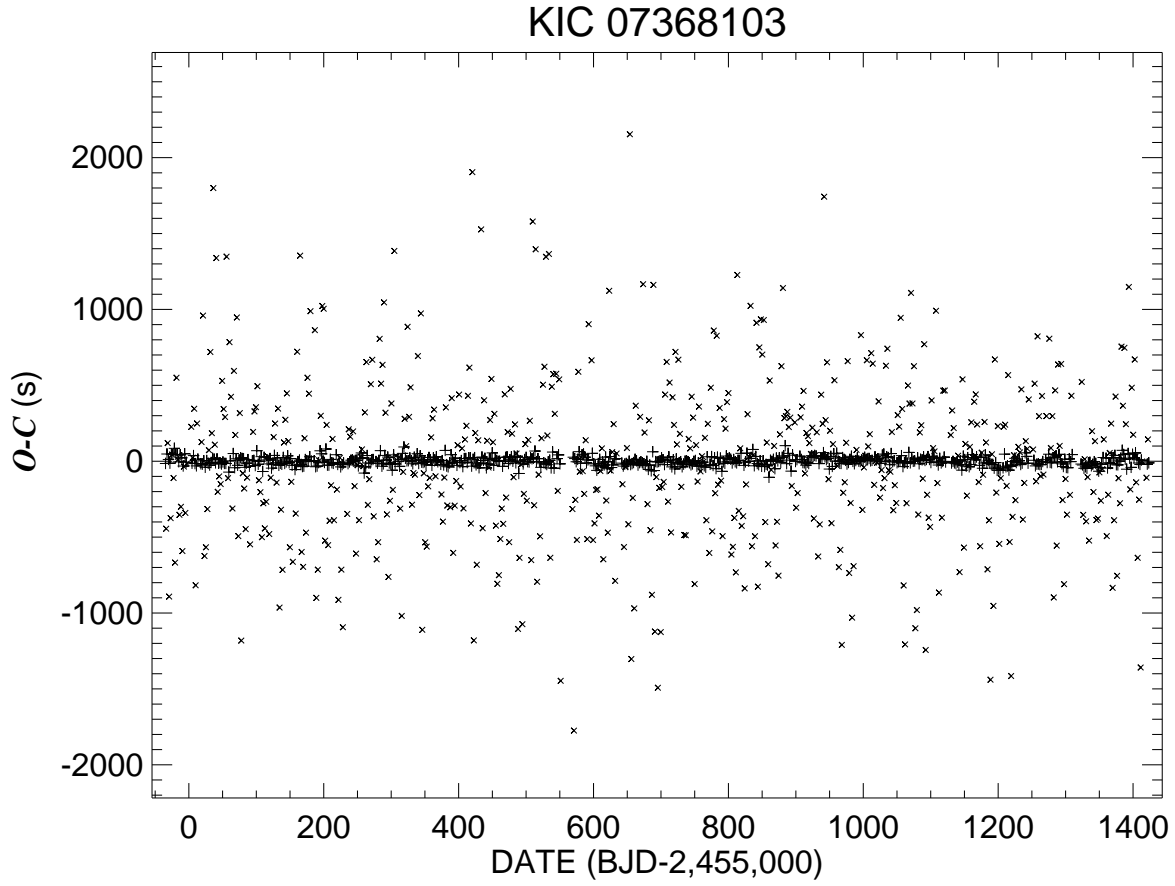


Fig. 1.18.— The observed minus calculated eclipse times relative to a linear ephemeris. The primary and secondary eclipse times are indicated by + and \times symbols, respectively.

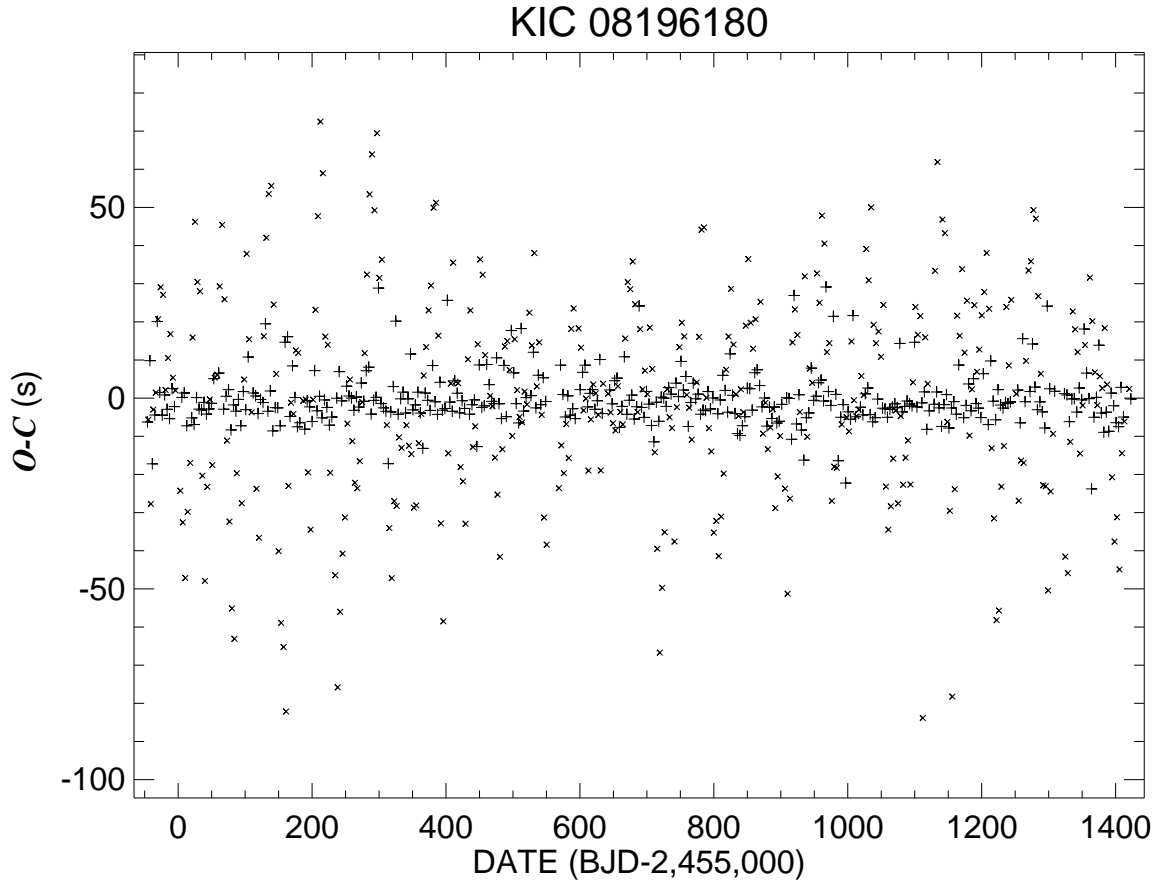


Fig. 1.19.— The observed minus calculated eclipse times relative to a linear ephemeris. The primary and secondary eclipse times are indicated by + and × symbols, respectively.

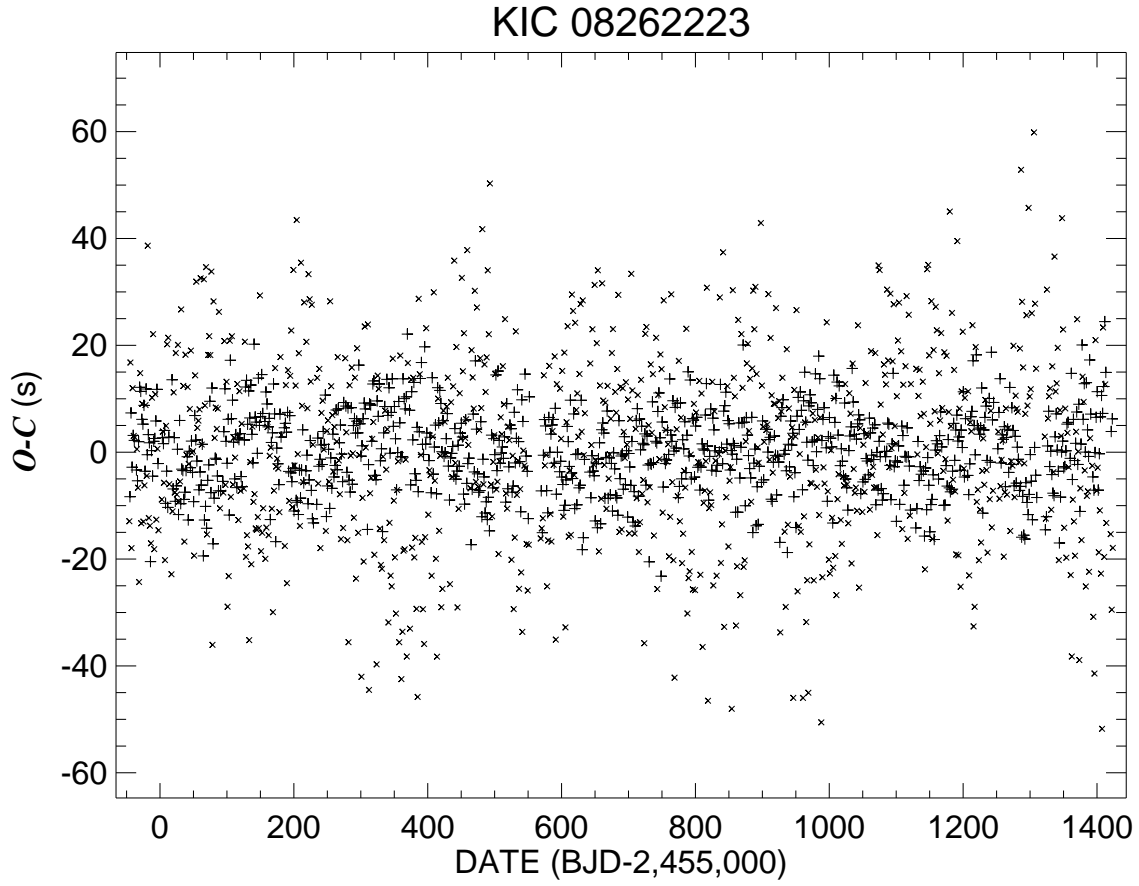


Fig. 1.20.— The observed minus calculated eclipse times relative to a linear ephemeris. The primary and secondary eclipse times are indicated by + and \times symbols, respectively.

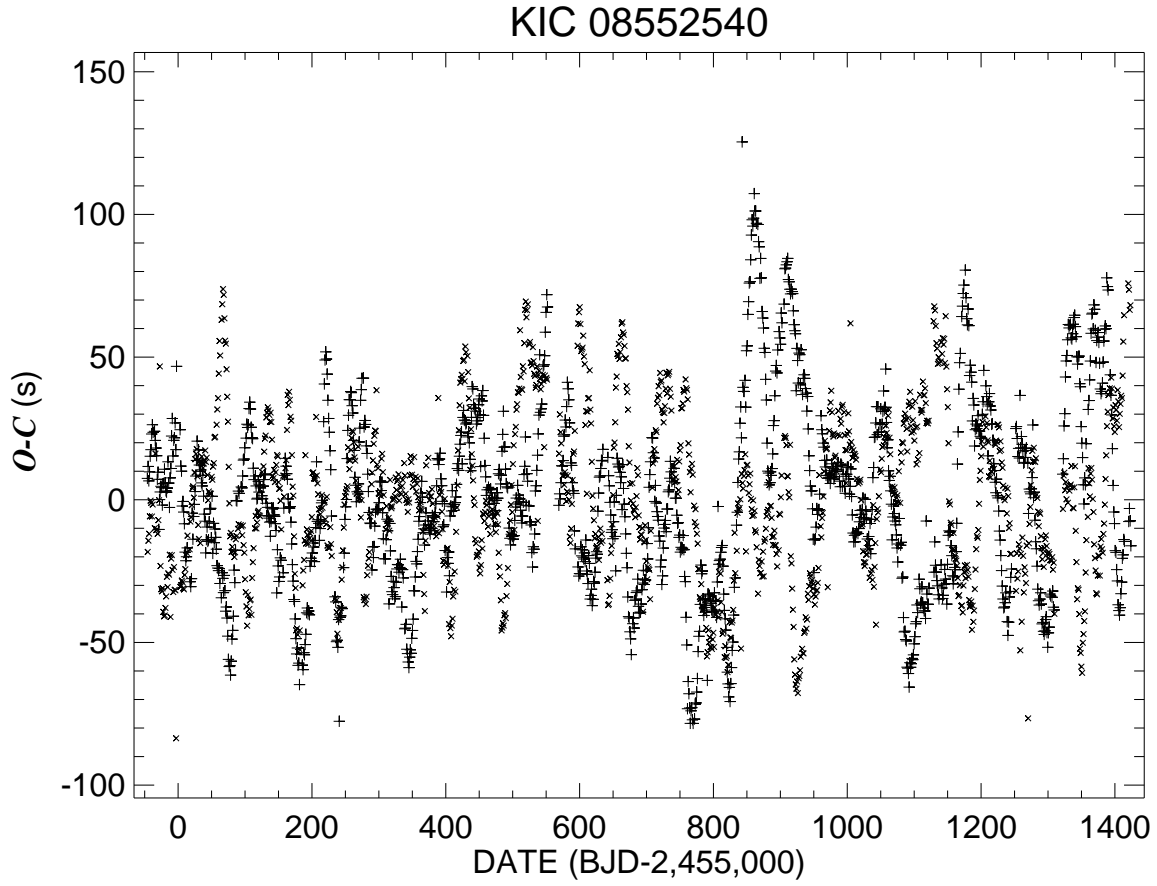


Fig. 1.21.— The observed minus calculated eclipse times relative to a linear ephemeris. The primary and secondary eclipse times are indicated by + and \times symbols, respectively.

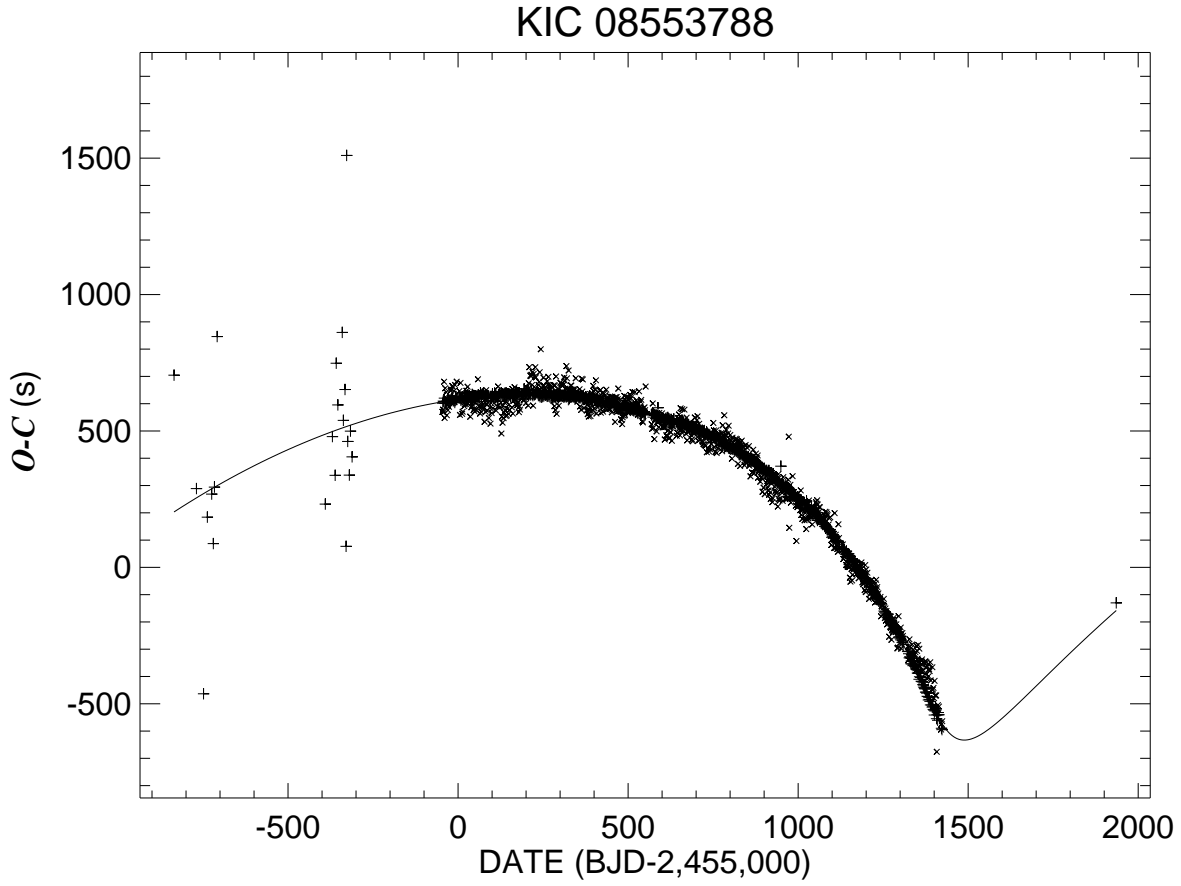


Fig. 1.22.— The observed minus calculated eclipse times relative to a linear ephemeris. The primary and secondary eclipse times are indicated by + and × symbols, respectively.

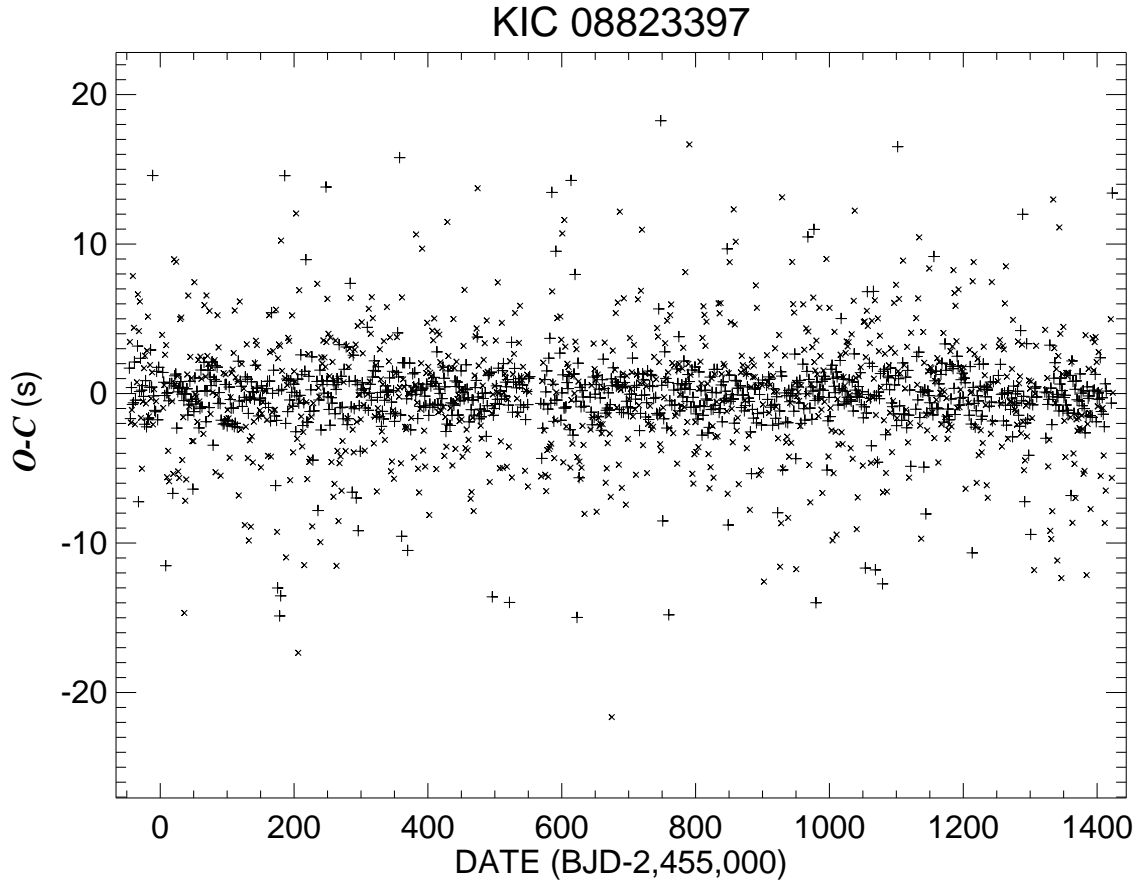


Fig. 1.23.— The observed minus calculated eclipse times relative to a linear ephemeris. The primary and secondary eclipse times are indicated by + and × symbols, respectively.

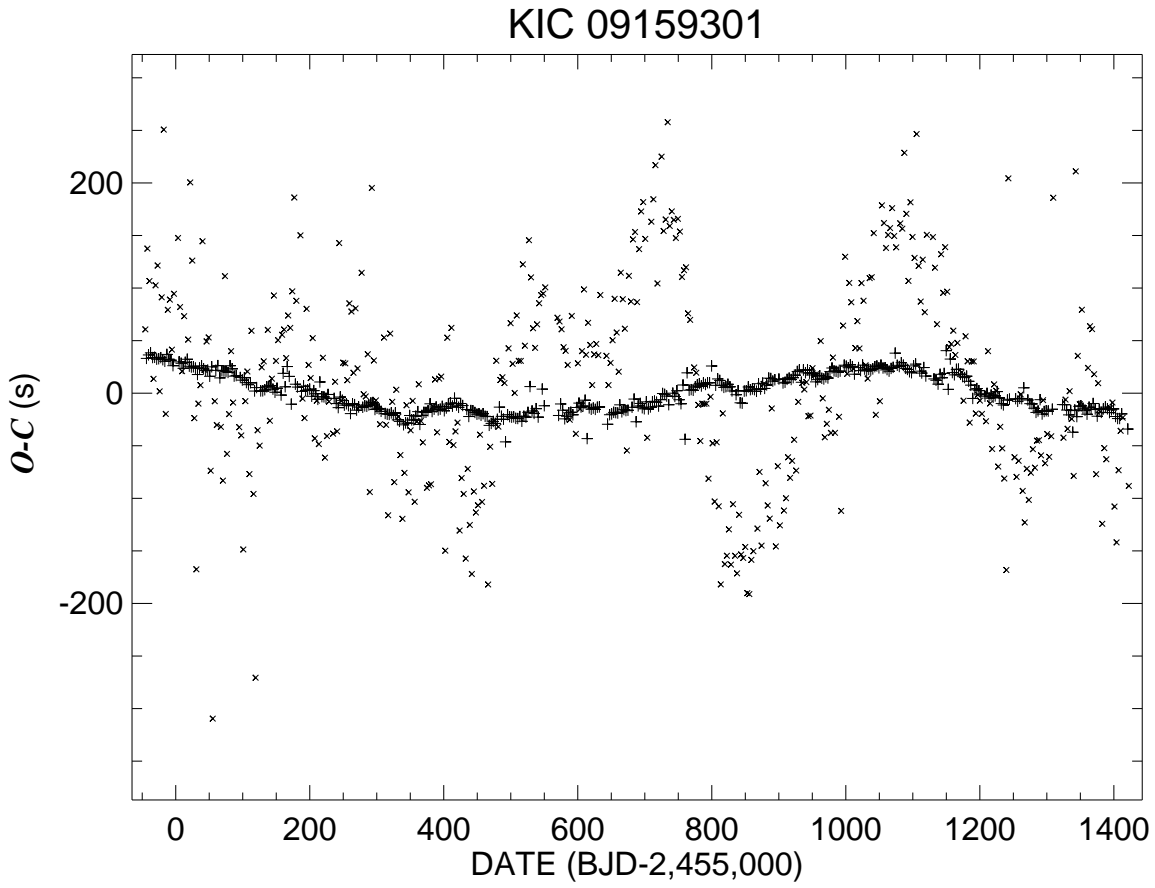


Fig. 1.24.— The observed minus calculated eclipse times relative to a linear ephemeris. The primary and secondary eclipse times are indicated by + and × symbols, respectively.

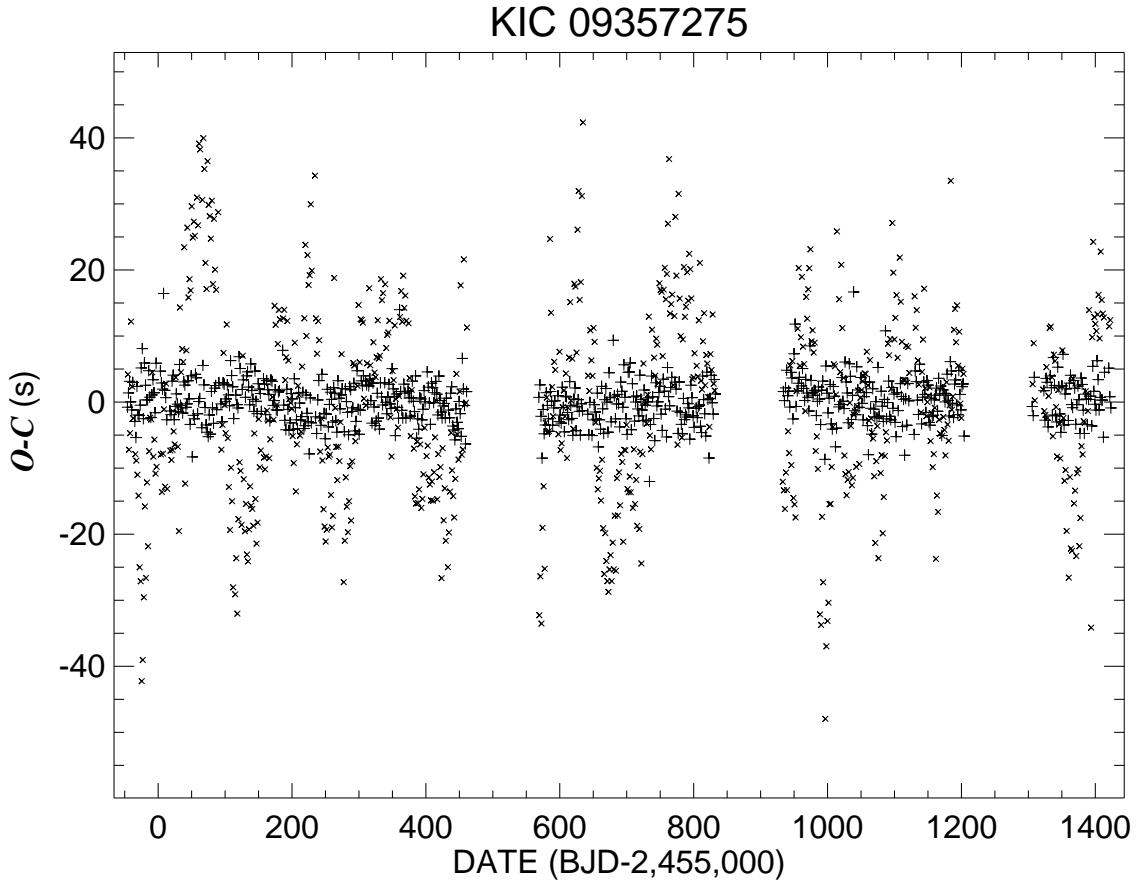


Fig. 1.25.— The observed minus calculated eclipse times relative to a linear ephemeris. The primary and secondary eclipse times are indicated by + and × symbols, respectively.

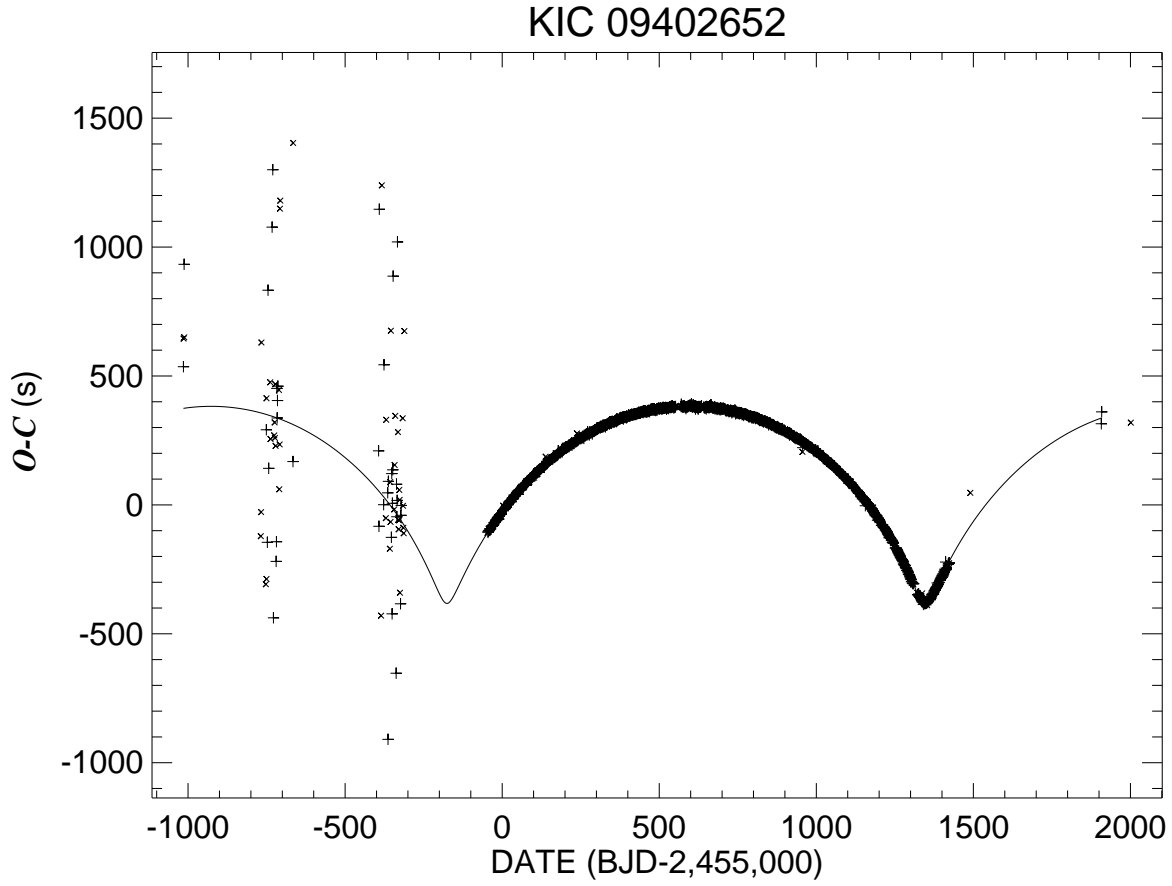


Fig. 1.26.— The observed minus calculated eclipse times relative to a linear ephemeris. The primary and secondary eclipse times are indicated by + and × symbols, respectively.

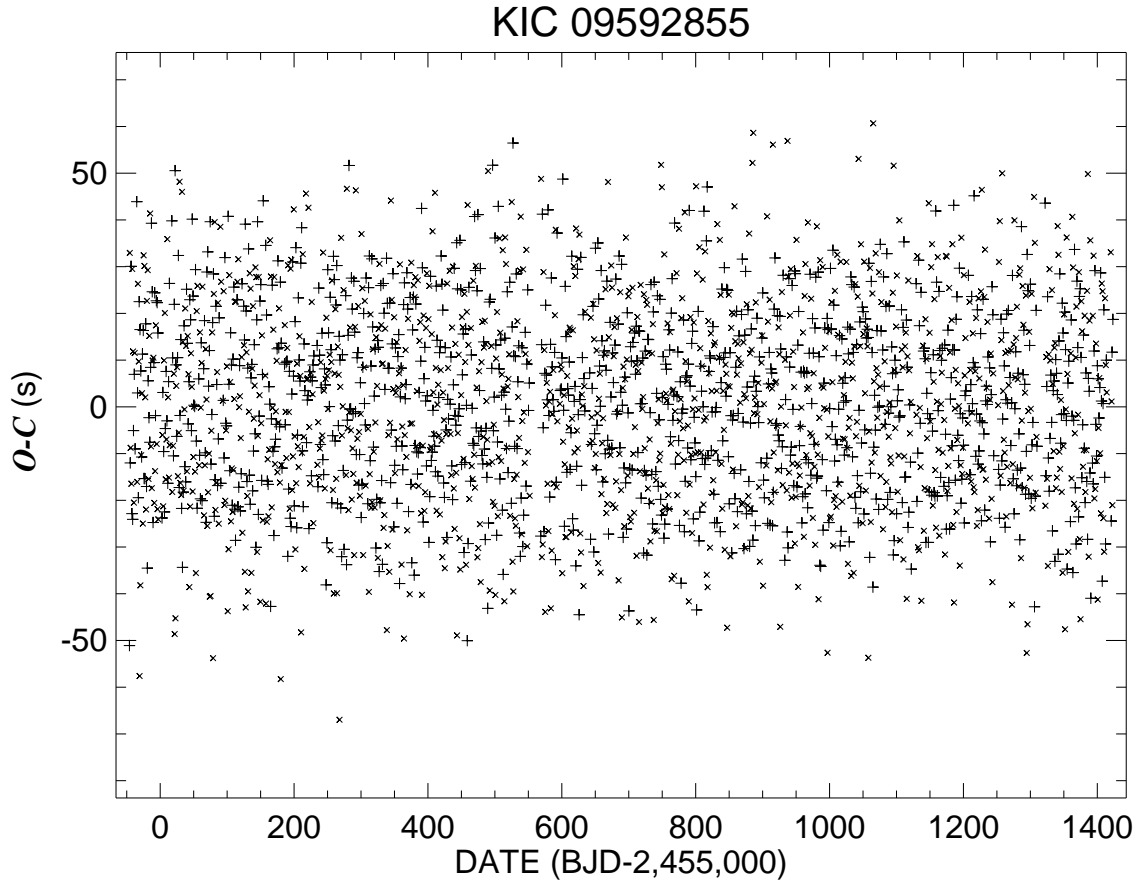


Fig. 1.27.— The observed minus calculated eclipse times relative to a linear ephemeris. The primary and secondary eclipse times are indicated by + and \times symbols, respectively.

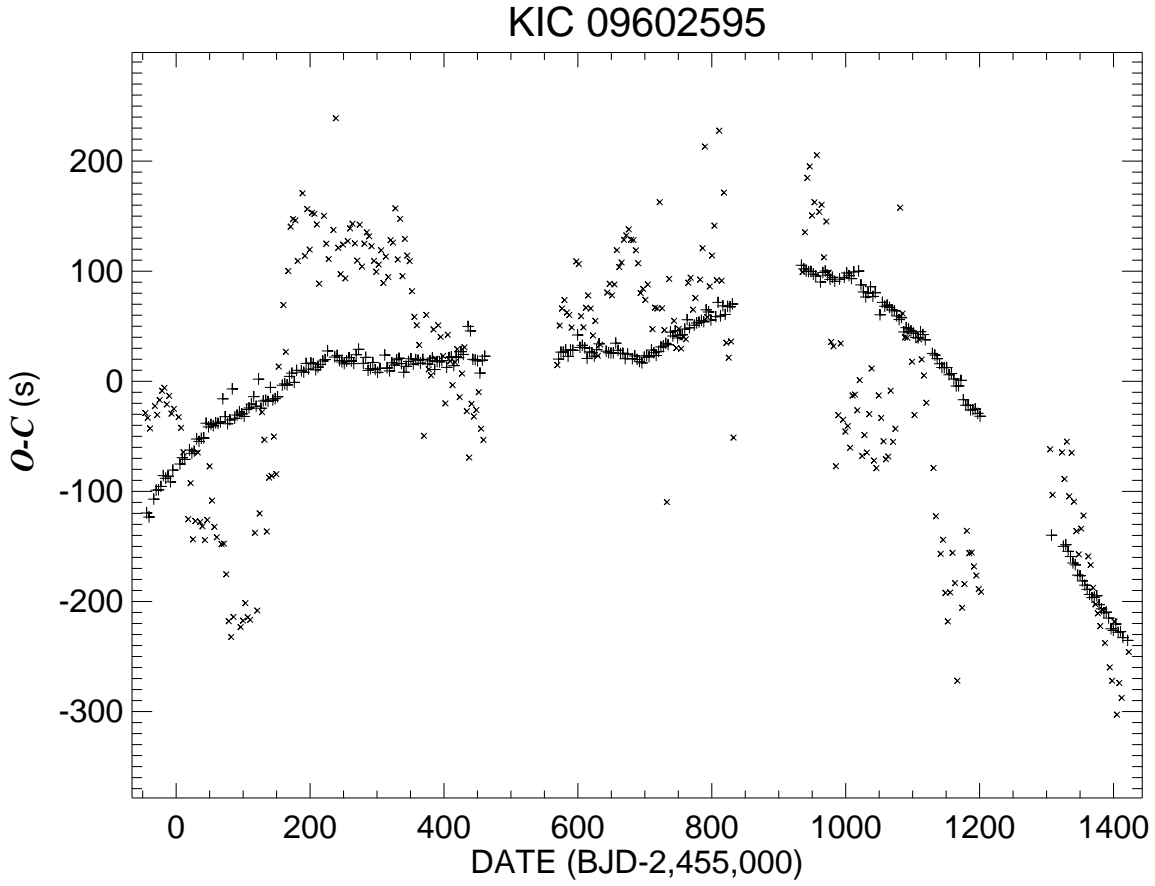


Fig. 1.28.— The observed minus calculated eclipse times relative to a linear ephemeris. The primary and secondary eclipse times are indicated by + and \times symbols, respectively.

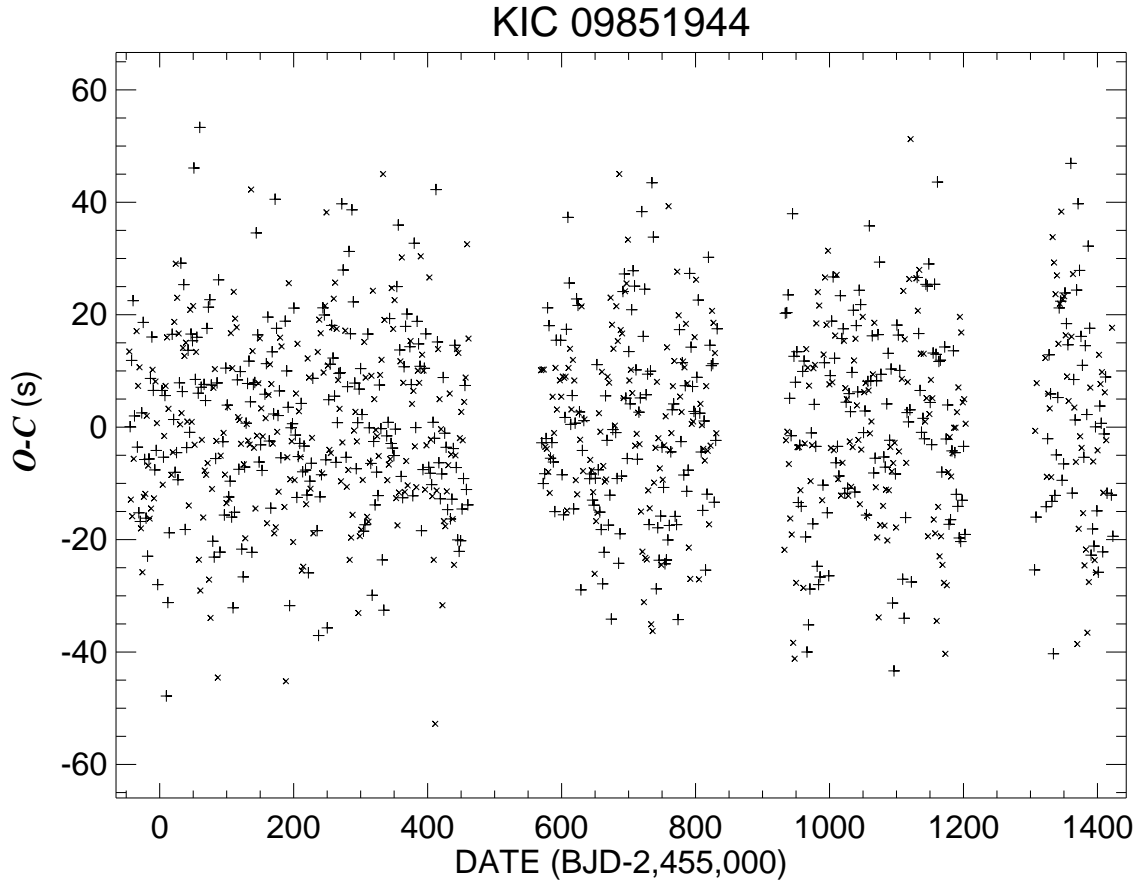


Fig. 1.29.— The observed minus calculated eclipse times relative to a linear ephemeris. The primary and secondary eclipse times are indicated by + and × symbols, respectively.

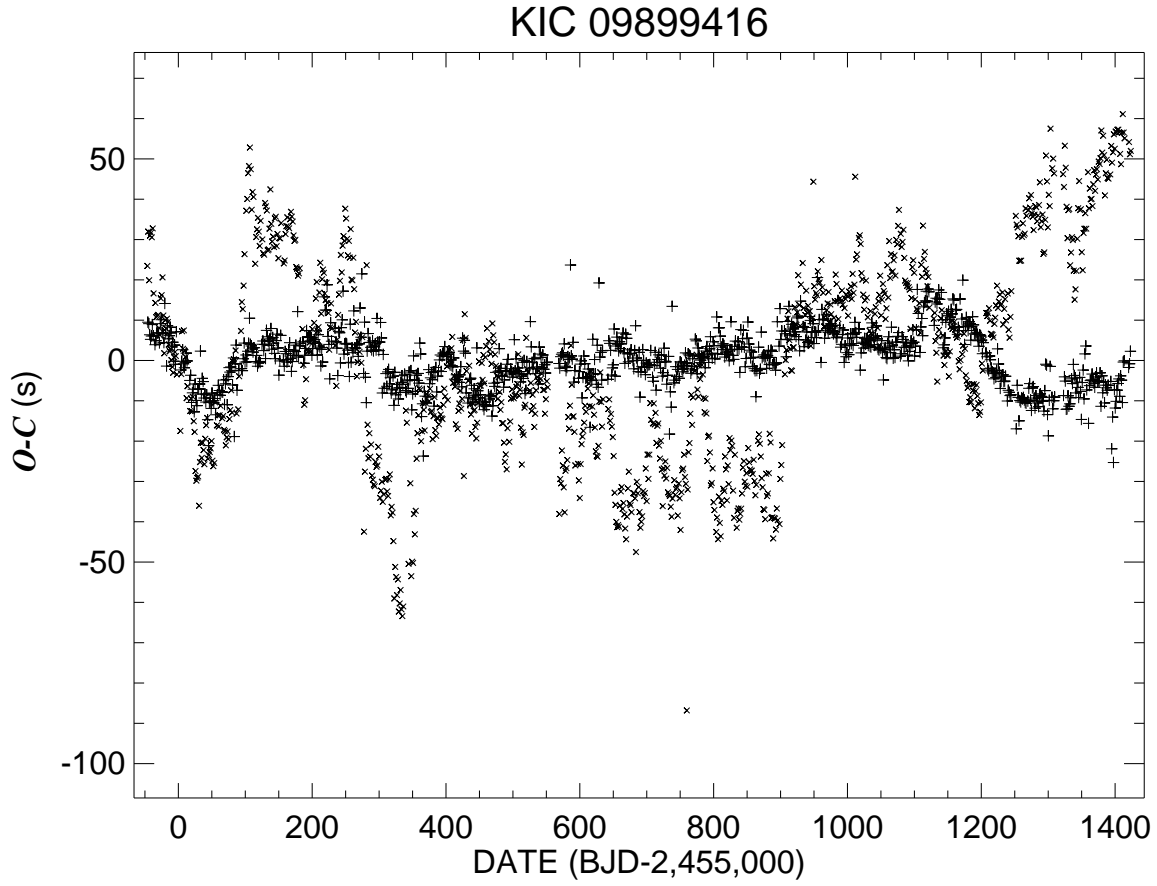


Fig. 1.30.— The observed minus calculated eclipse times relative to a linear ephemeris. The primary and secondary eclipse times are indicated by + and \times symbols, respectively.

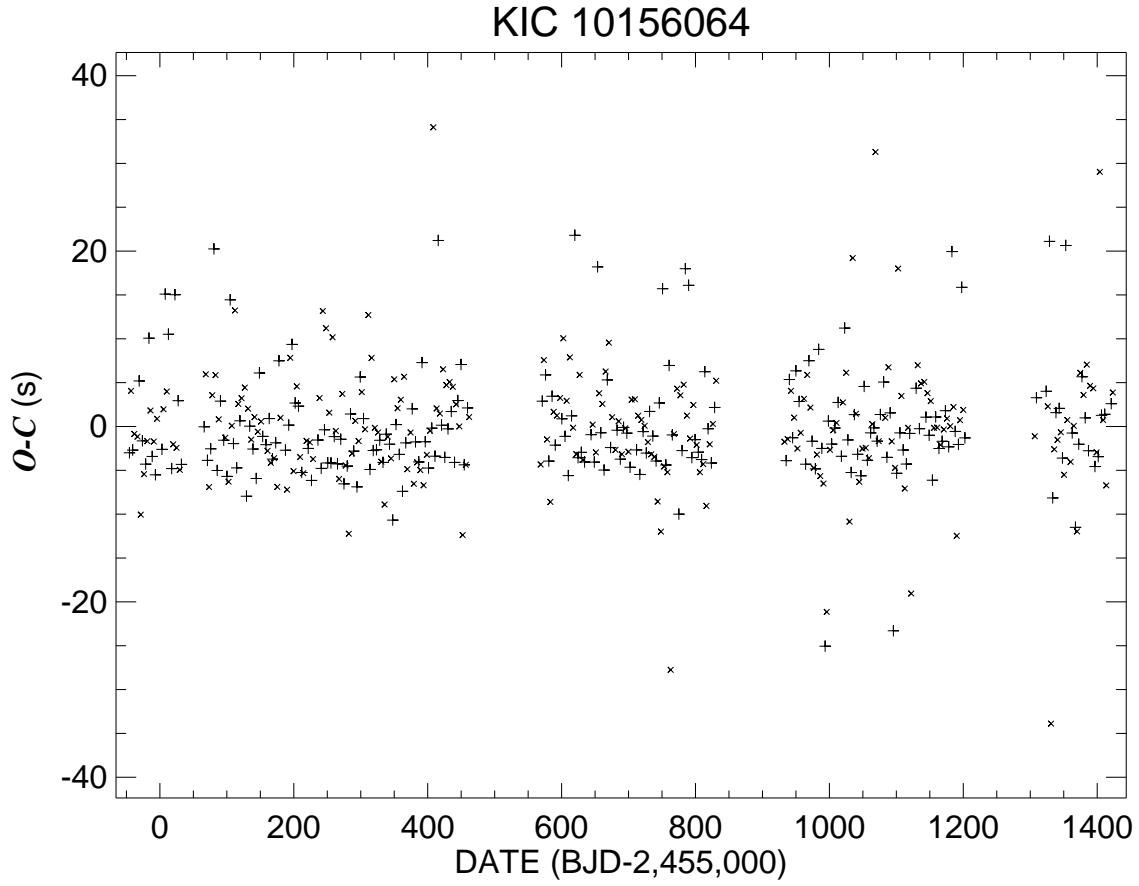


Fig. 1.31.— The observed minus calculated eclipse times relative to a linear ephemeris. The primary and secondary eclipse times are indicated by + and \times symbols, respectively.

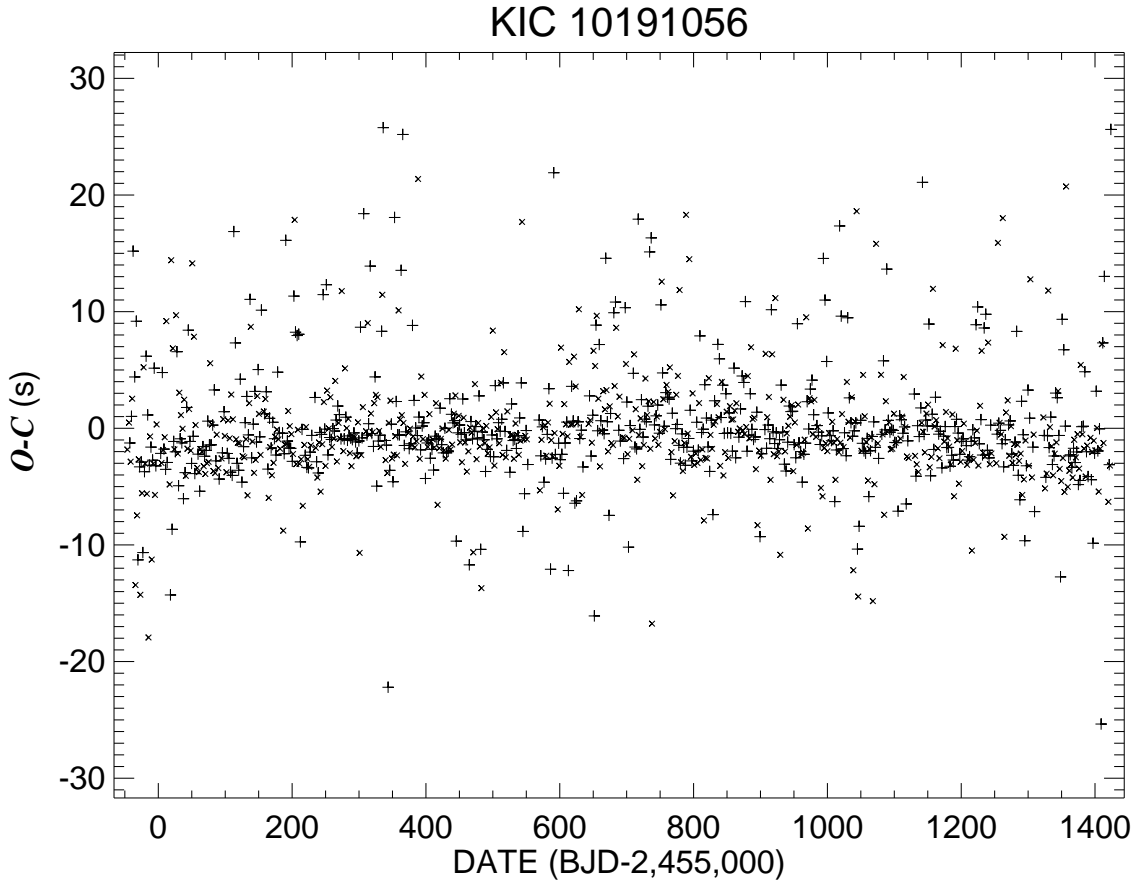


Fig. 1.32.— The observed minus calculated eclipse times relative to a linear ephemeris. The primary and secondary eclipse times are indicated by + and × symbols, respectively.

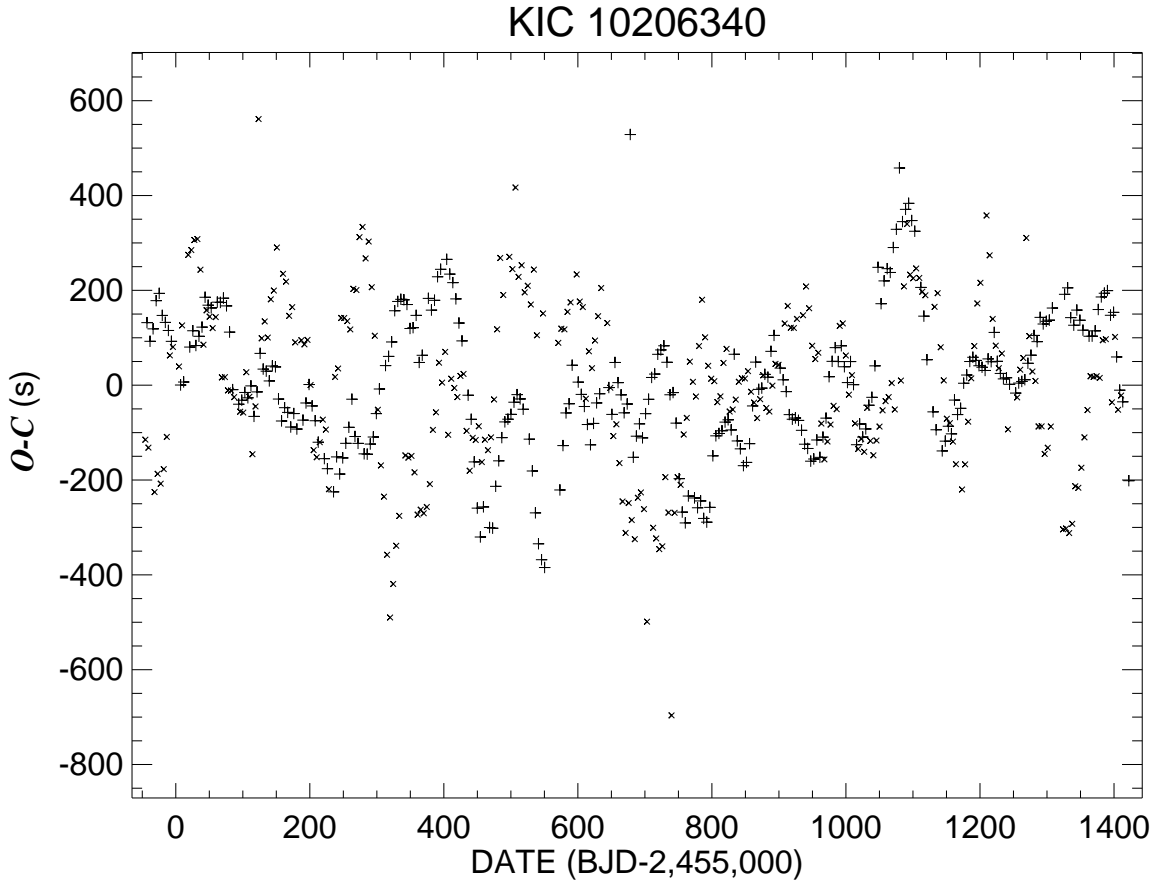


Fig. 1.33.— The observed minus calculated eclipse times relative to a linear ephemeris. The primary and secondary eclipse times are indicated by + and \times symbols, respectively.

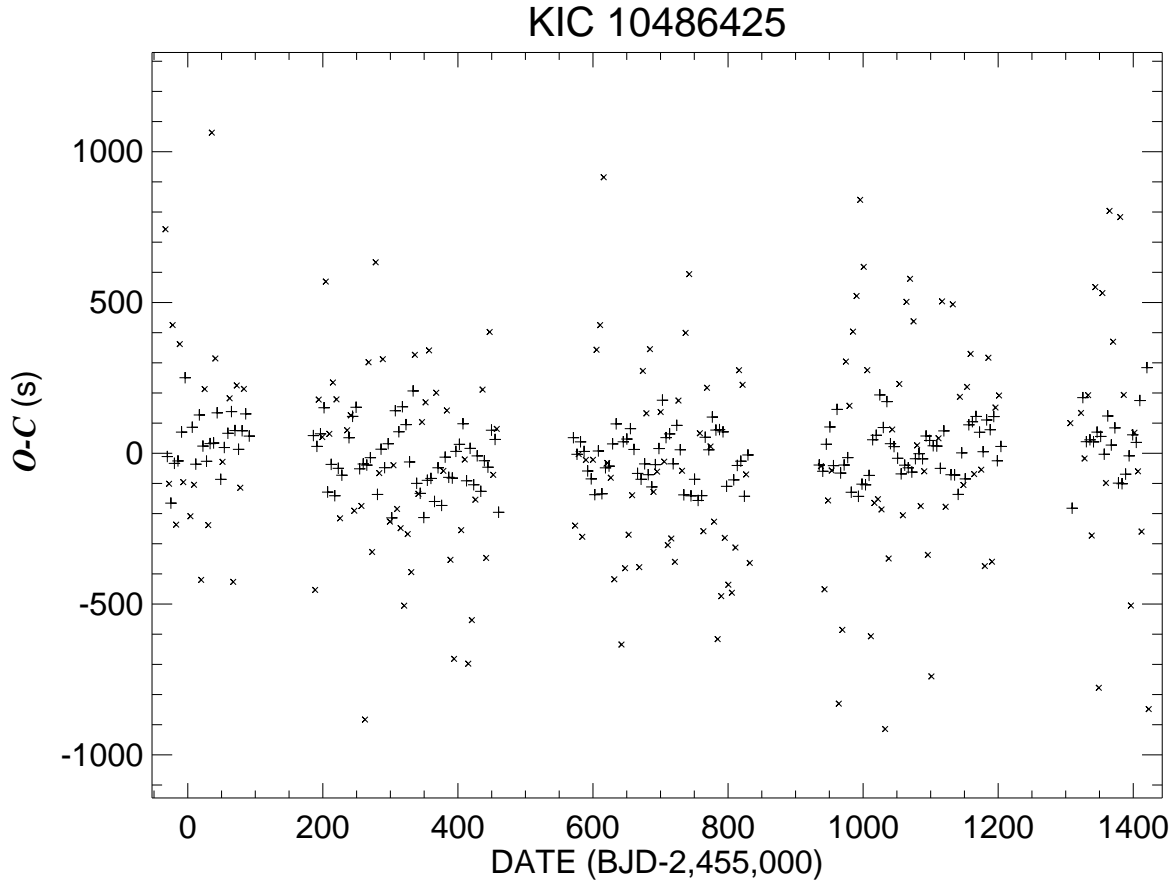


Fig. 1.34.— The observed minus calculated eclipse times relative to a linear ephemeris. The primary and secondary eclipse times are indicated by + and \times symbols, respectively.

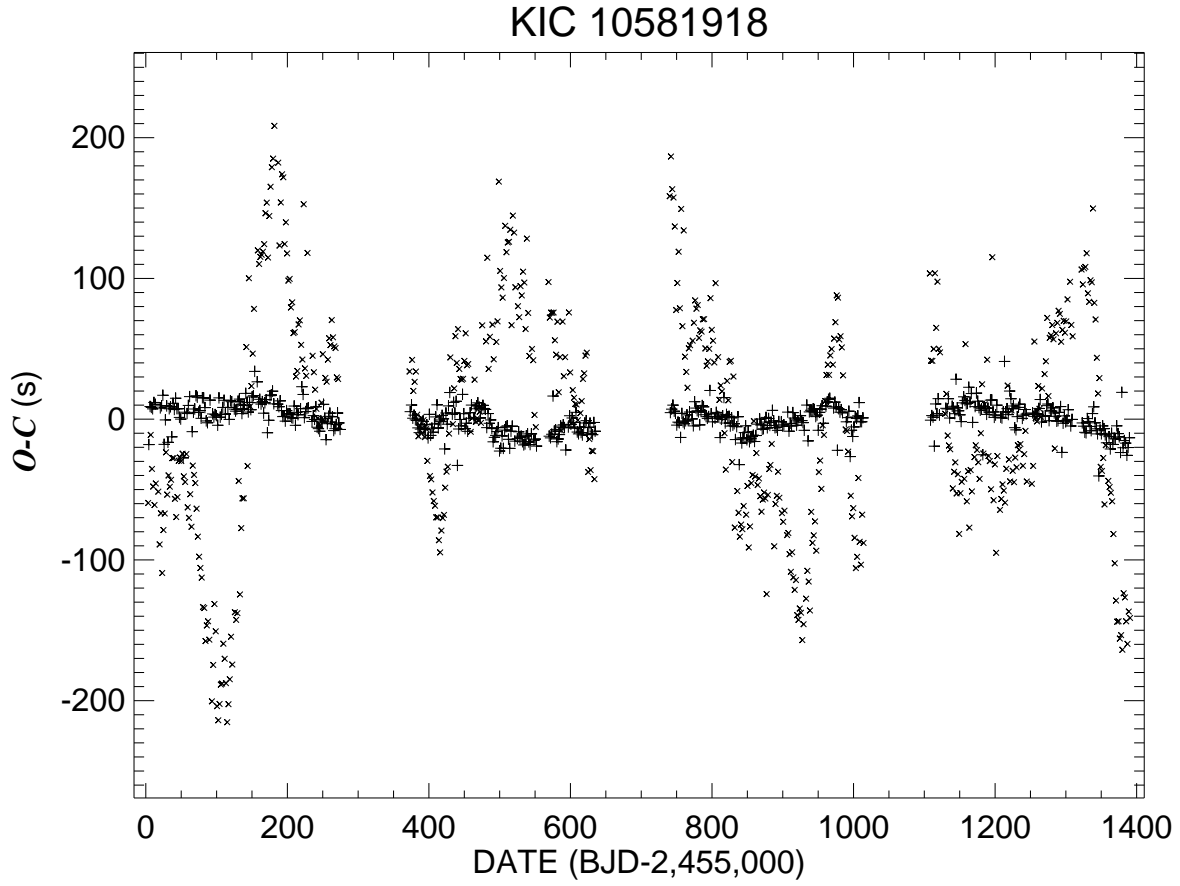


Fig. 1.35.— The observed minus calculated eclipse times relative to a linear ephemeris. The primary and secondary eclipse times are indicated by + and \times symbols, respectively.

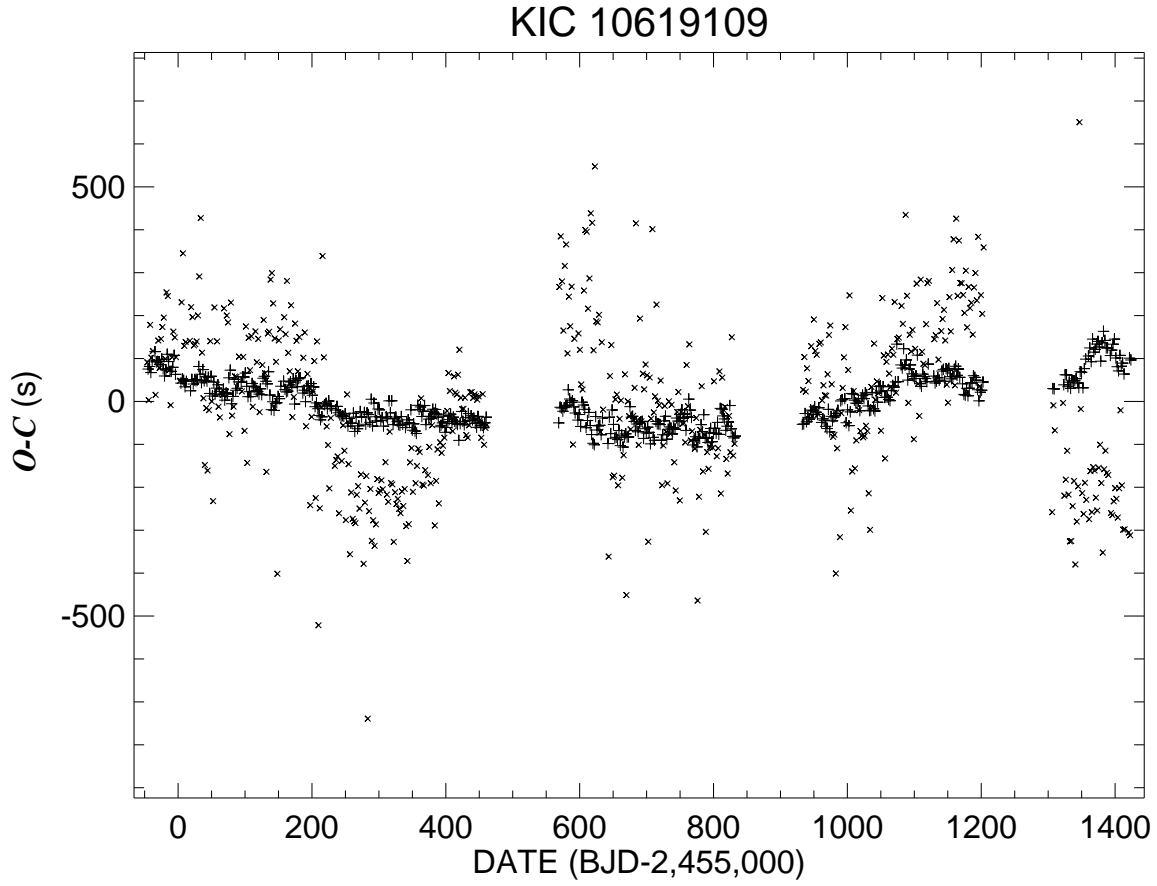


Fig. 1.36.— The observed minus calculated eclipse times relative to a linear ephemeris. The primary and secondary eclipse times are indicated by + and × symbols, respectively.

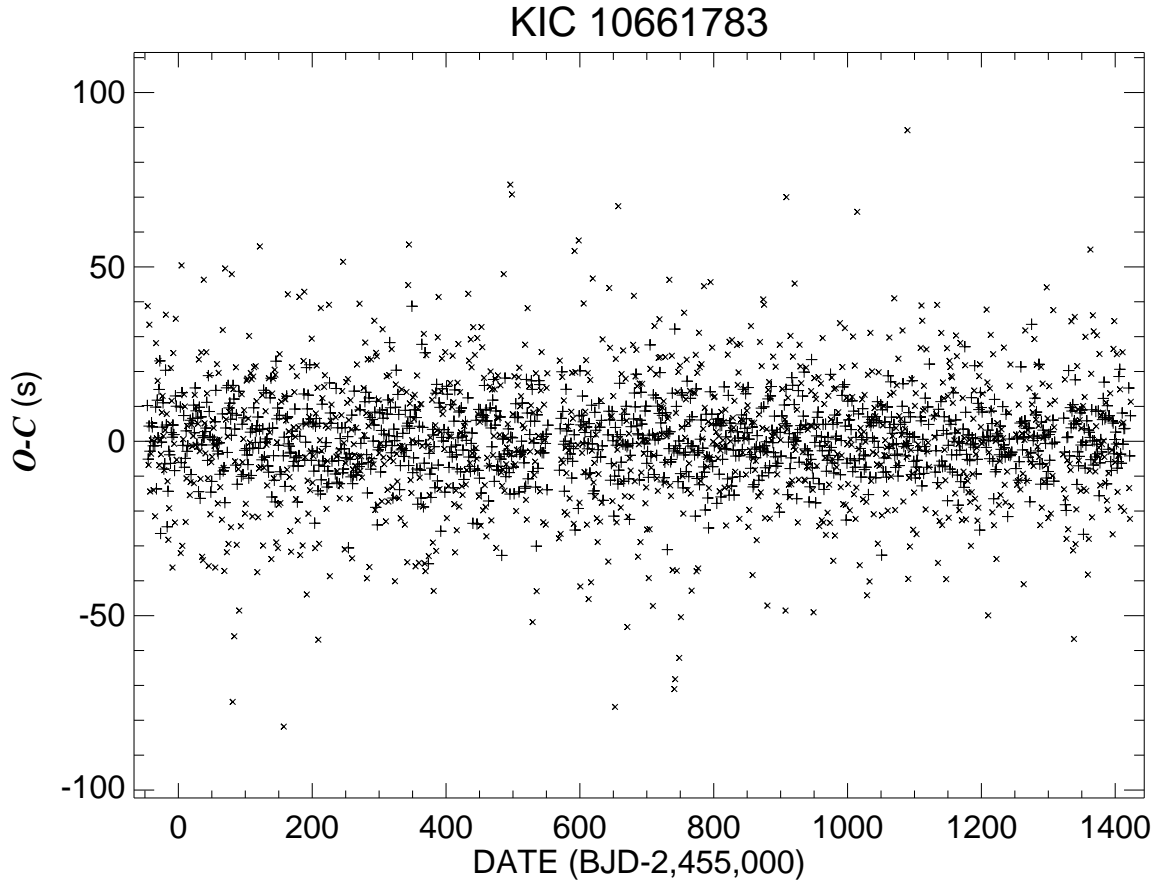


Fig. 1.37.— The observed minus calculated eclipse times relative to a linear ephemeris. The primary and secondary eclipse times are indicated by + and \times symbols, respectively.

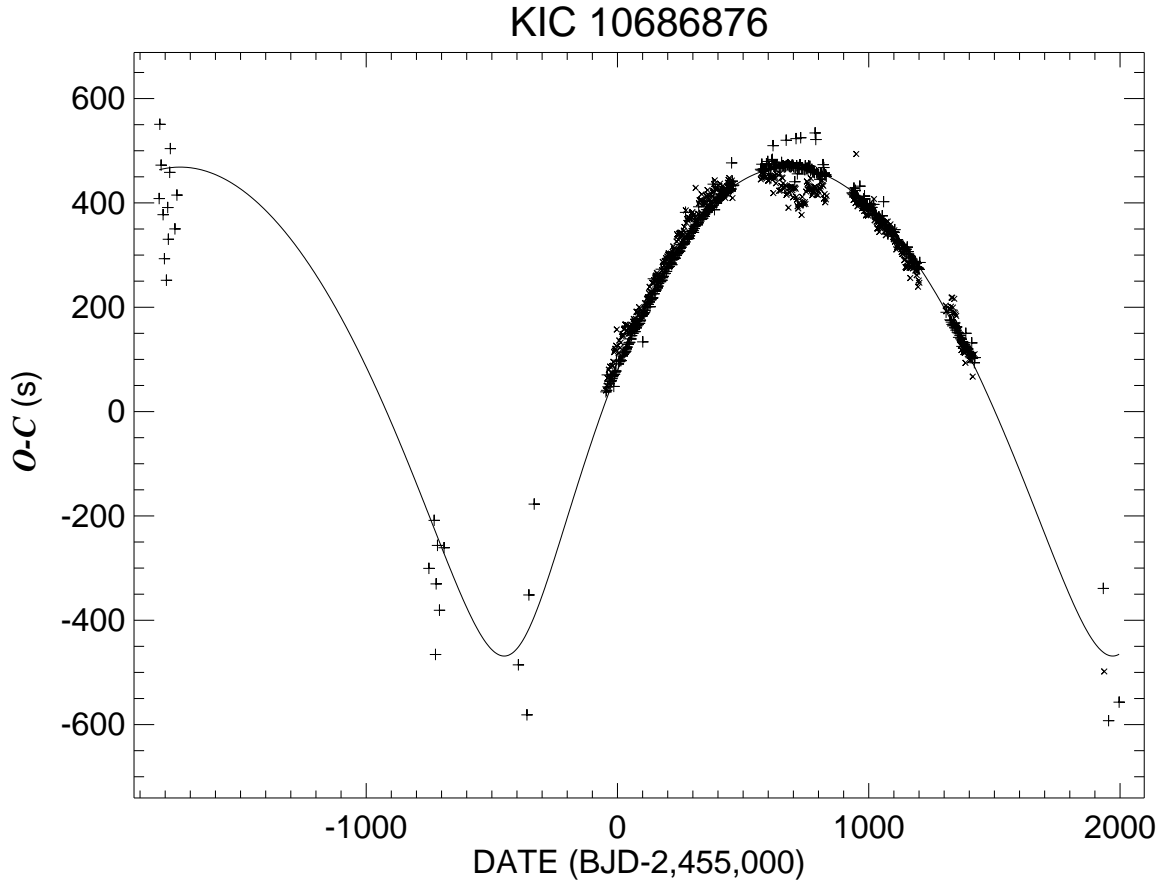


Fig. 1.38.— The observed minus calculated eclipse times relative to a linear ephemeris. The primary and secondary eclipse times are indicated by + and × symbols, respectively.

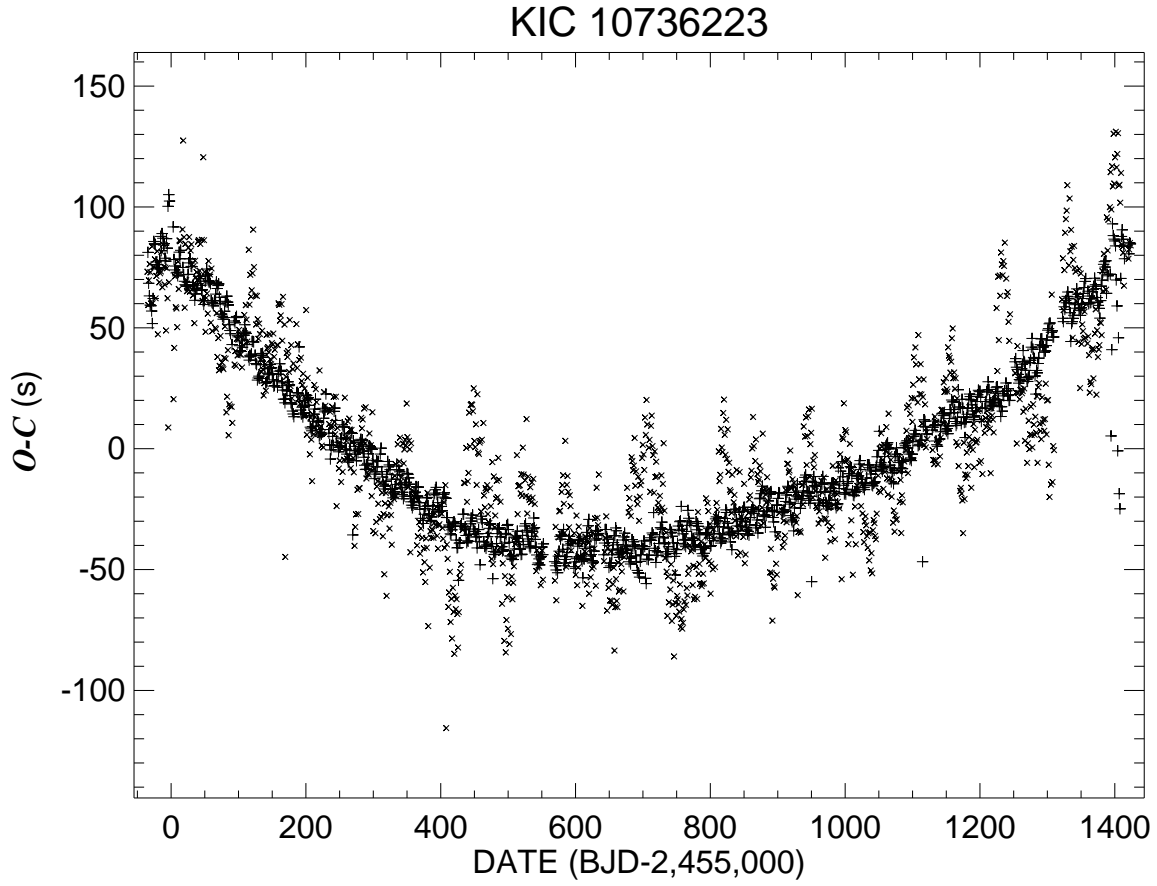


Fig. 1.39.— The observed minus calculated eclipse times relative to a linear ephemeris. The primary and secondary eclipse times are indicated by + and × symbols, respectively.

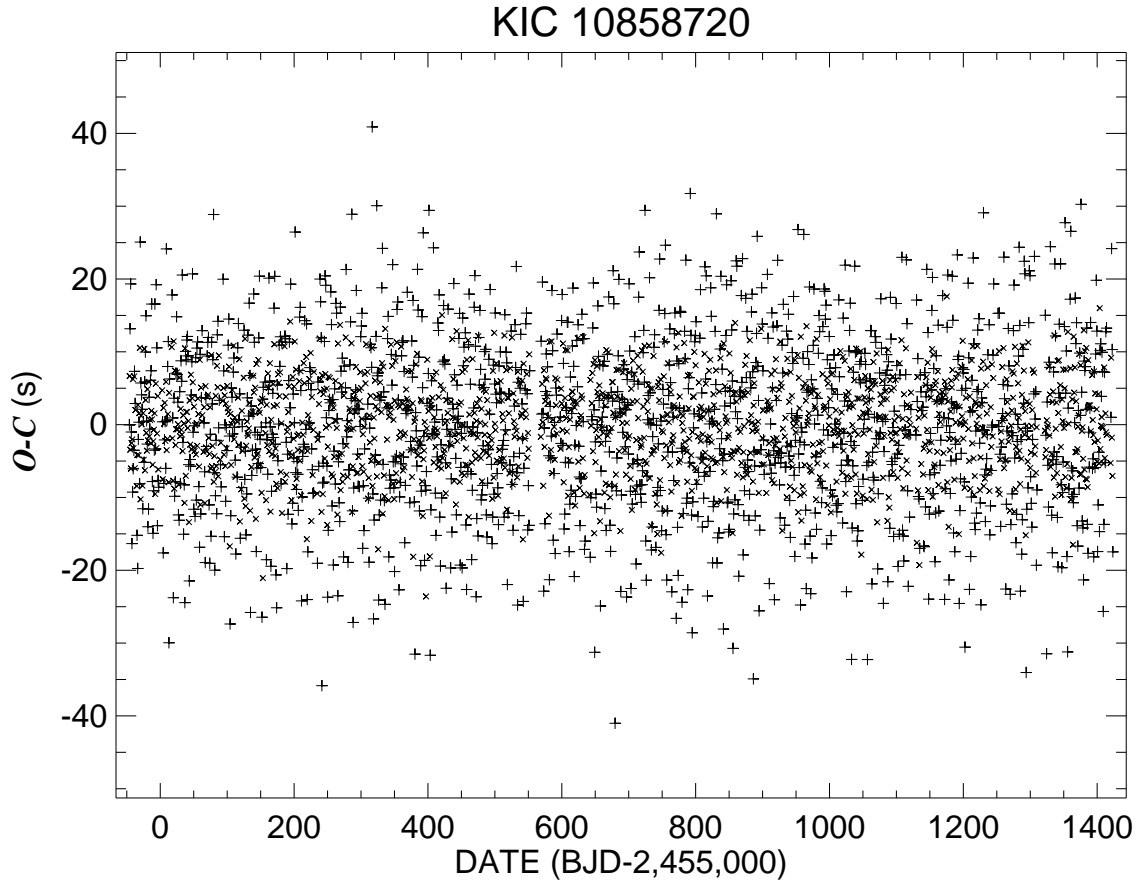


Fig. 1.40.— The observed minus calculated eclipse times relative to a linear ephemeris. The primary and secondary eclipse times are indicated by + and \times symbols, respectively.

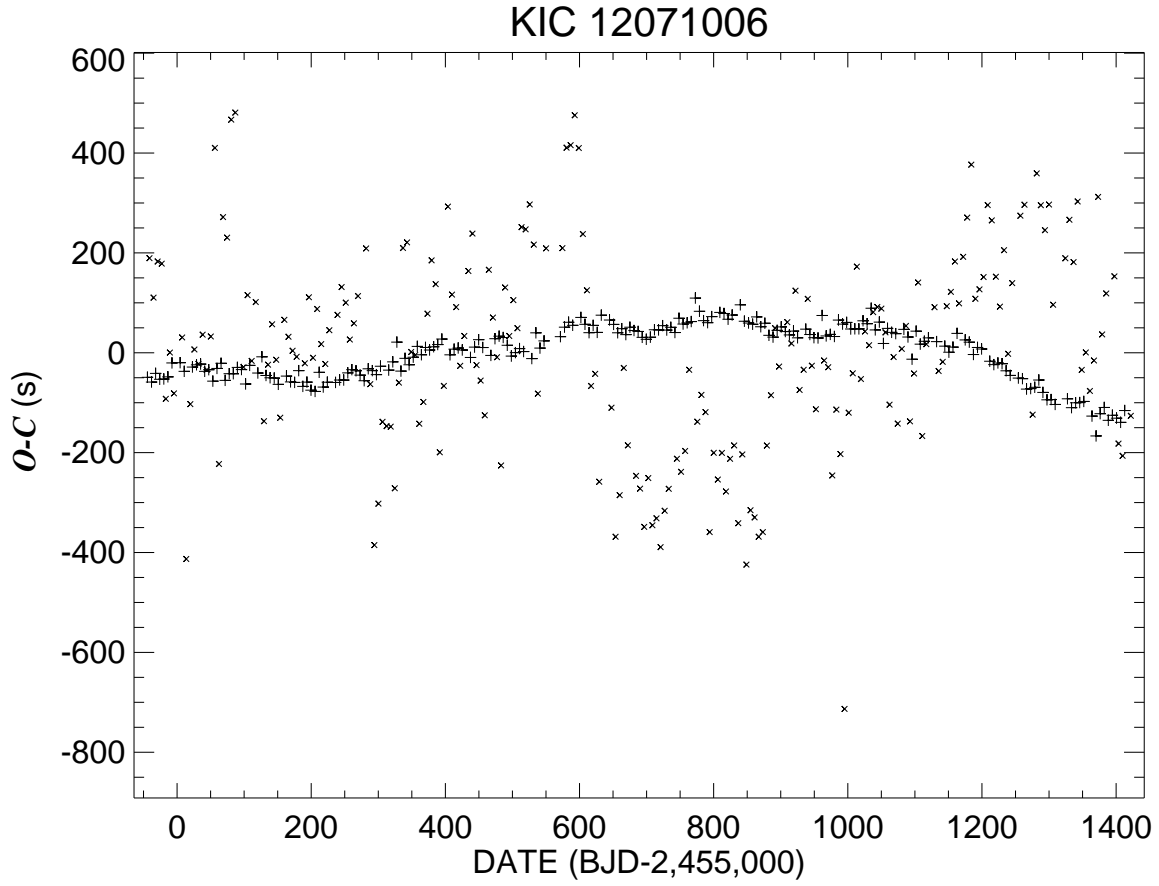


Fig. 1.41.— The observed minus calculated eclipse times relative to a linear ephemeris. The primary and secondary eclipse times are indicated by + and × symbols, respectively.